JGR Biogeosciences

RESEARCH ARTICLE
10.1029/2020JG005658

Influence of Vertical Heterogeneities in the Canopy Microenvironment on Interannual Variability of Carbon Uptake in Temperate Deciduous Forests

M. C. Wozniak[1,2], G. B. Bonan[3], G. Keppel-Aleks[1], and A. L. Steiner[1]

[1]Department of Climate and Space Sciences and Engineering, University of Michigan, Ann Arbor, MI, USA, [2]Now at Program in Atmospheric and Oceanic Sciences, Princeton University, Princeton, NJ, USA, [3]National Center for Atmospheric Research, Boulder, CO, USA

Key Points:
- Explicitly simulated leaf area and microclimatic profiles do not affect gross primary productivity (GPP) interannual variability compared to a "big-leaf" simplification
- Multilayer plant hydraulics lead to vertically varying water stress, altering leaf-layer responses to interannual climate variations
- All model simulations underestimate hourly GPP compared to FLUXNET estimates, adversely impacting simulated GPP interannual variability

Supporting Information:
- Supporting Information S1

Correspondence to:
M. C. Wozniak,
mwozniak@princeton.edu

Citation:
Wozniak, M. C., Bonan, G. B., Keppel-Aleks, G., & Steiner, A. L. (2020). Influence of vertical heterogeneities in the canopy microenvironment on interannual variability of carbon uptake in temperate deciduous forests. *Journal of Geophysical Research: Biogeosciences*, *125*, e2020JG005658. https://doi.org/10.1029/2020JG005658

Received 19 JAN 2020
Accepted 30 JUN 2020
Accepted article online 28 JUL 2020

Author Contributions:
Conceptualization: G. Keppel-Aleks, A. L. Steiner
Funding acquisition: G. Keppel-Aleks, A. L. Steiner
Project administration: G. Keppel-Aleks, A. L. Steiner
Resources: G. Keppel-Aleks, A. L. Steiner
Software: G. B. Bonan
Supervision: G. B. Bonan, G. Keppel-Aleks, A. L. Steiner
Writing – review & editing: G. B. Bonan, G. Keppel-Aleks, A. L. Steiner

Abstract Vegetation structure and function are key design choices in terrestrial models that affect the relationship between carbon uptake and environmental drivers. Here, we investigate how representing canopy vertical structure in a terrestrial biosphere model—that is, micrometeorological, leaf area, and leaf water profiles—influences carbon uptake at five U.S. temperate deciduous forest sites in July. Specifically, we test whether the interannual variability (IAV) of gross primary productivity (GPP) responds differently to four abiotic environmental drivers—air temperature, relative humidity, incoming shortwave radiation, and soil moisture—using either a Community Land Model multilayer canopy model (CLM-ml) or a big-leaf model (CLM4.5/CLM5). We conclude that vertical leaf area and microclimatic profiles (temperature, humidity, and wind) do not impact GPP IAV compared to a single-layer model when plant hydraulics is excluded. However, with a mechanistic representation of plant hydraulics there is vertically varying water stress in CLM-ml, and the sensitivity of carbon uptake to particular climate variables changes with height, resulting in dampened canopy-scale GPP IAV relative to CLM4.5. Dampening is due to both a reduced dependence on soil moisture and opposing climatic forcing on different leaf layers. Such dampening is not evident in the single-layer representation of plant hydraulic water stress implemented in the recently released CLM5. Overall, both model representations of the canopy fail to accurately simulate observed GPP IAV and this may be related by their inability to capture the upper range of observed hourly GPP and diffuse light-GPP relationships that cannot be resolved by canopy structure alone.

1. Introduction

Interannual variability (IAV) in the growth rate of atmospheric CO_2 concentrations is largely dependent on the variability of the land sink (Keeling et al., 1995; le Quéré et al., 2017; Nevison et al., 2008; Schimel et al., 2001), and the land sink is closely coupled to climate variability (Ahlström et al., 2015; Beer et al., 2010; Fu et al., 2017; Poulter et al., 2014; Rödenbeck et al., 2018; Sitch et al., 2015). A quantitative understanding of the relationship between climate variations and the land sink response is therefore crucial for accurate prediction of carbon-climate feedbacks. Because photosynthesis represents the pathway by which carbon enters terrestrial ecosystems, understanding the sensitivity of this process to environmental drivers is necessary to constrain the terrestrial carbon sink (Anav et al., 2015). The environmental drivers of photosynthesis—temperature, moisture, and radiation—often covary. For example, drought conditions usually reflect both low precipitation and high temperature, while above-average precipitation likely cooccurs with high cloud cover, which reduces radiation. These covariances make it difficult to unambiguously attribute variations in gross primary productivity (GPP) to the underlying driver.

Terrestrial biosphere models are one way the disambiguation of carbon cycle processes can be achieved. Earth system models (ESMs) equipped with terrestrial biosphere models can simulate the evolution of the terrestrial carbon sink under climate change and the sink's coupling with climate (Anav et al., 2013; Arora et al., 2013). However, modeling estimates of the IAV of the terrestrial carbon sink diverge due to the uncertainty in terrestrial model processes (Bonan & Doney, 2018; Keenan et al., 2012). Some of this uncertainty results from simplifications in representing ecological processes within land models. For

example, most ESM land components simulate the vegetation canopy as a simplified single bulk leaf layer, or "big-leaf," that exchanges mass and energy with the atmosphere (Sinclair et al., 1976). In reality, vertical structure in the tall canopies of forests may influence the response of carbon uptake to variability in these drivers, including on the interannual scale.

Forest canopies, including temperate deciduous canopies, exhibit considerable structural heterogeneity from the top to the bottom that impacts the within-canopy physical environment, particularly light extinction, microclimate, and leaf water stress. Leaf area density, leaf angle, and other canopy architectural traits (e.g., clumping) also vary with height in forest canopies (Niinemets, 1998; Parker et al., 1989; Walcroft et al., 2005; Zhao et al., 2011). Such vertical architectural heterogeneity can affect radiation extinction from successive canopy shading and potentially lead to diurnal, seasonal, or spatial differences in carbon uptake depending on canopy structure (Funk & Lerdau, 2004; Koike et al., 2001; Niinemets & Valladares, 2004; Parker et al., 2005). The interactions between canopy architecture, the varied light environment, and within-canopy turbulence produce a vertically varied microclimate (Eliáš et al., 1989; Flerchinger et al., 2015) capable of moderating weather and climatic extremes (Carlson & Groot, 1997; Chen et al., 1999; de Frenne et al., 2013; Rambo & North, 2009; von Arx et al., 2012). Because photosynthesis is tightly coupled with meteorological conditions, carbon uptake in canopies is sensitive to vertical light and meteorological gradients and the interactions between such gradients, particularly during meteorological extremes (Niinemets & Valladares, 2004).

Vertically resolved multilayer canopy models have been applied to vegetation-atmosphere carbon fluxes in forests and other plant canopies to resolve the impacts of vertical heterogeneity in canopy architecture and environmental conditions (Baldocchi et al., 2002; Bonan et al., 2014, 2018; Chang & Chen, 2018; Drewry et al., 2010; Walcroft et al., 2005; Wu et al., 2003). For example, a recent study using the Advanced Canopy-Atmosphere-Soil Algorithm (ACASA) model concluded that resolved scalar profiles (temperature, humidity, and carbon dioxide) reduced canopy carbon uptake by an average of 10% and that the multilayer model improved simulated daily fluxes compared to a single layer model at sites where seasonal variability in canopy structure (leaf area index, LAI) was great (Chang & Chen, 2018). Drewry et al. (2010) and Wu et al. (2003) both analyzed the sensitivity of canopy CO_2 fluxes to meteorological conditions and found that modeled CO_2 flux was sensitive to vertical temperature gradient. Walcroft et al. (2005) found that vertically varied clumping (i.e., overlap of leaves) increased simulated canopy photosynthesis by 12% relative to randomly distributed leaves. Finally, Bonan et al. (2014) found that including vertically resolved plant hydraulics and water stress improved the simulated diurnal cycle of GPP in forests that were water stressed and postulated that vertical canopy profiles may be important for accurately simulating vegetation-atmosphere fluxes. These studies show that vertical representation in canopy models could be important to photosynthetic carbon uptake and its response to the environment.

Adding further complexity to a forest canopy is the hydraulic architecture of plants by which soil water is transferred to leaves to maintain moisture during photosynthesis (Tyree & Ewers, 1991). Plant hydraulic stress occurs when xylem water potential drops below a threshold that causes a loss in hydraulic conductivity within the plant. Observational studies show that plant hydraulic adaptation to water stress may be important for photosynthetic performance in relationship to water availability (Aranda et al., 2015; Taylor & Eamus, 2008; Zhang & Cao, 2009). Therefore, vegetation models may benefit from more realistic plant hydraulic trait-based carbon-water coupling, such as accounting for stomatal responses to reduced xylem pressure (e.g., Bonan et al., 2014). Plant hydraulic stress is not distributed evenly throughout the canopy, though, as water potential varies with the vertical canopy light gradient because of covarying leaf temperature and vapor pressure deficit (VPD; Hellkvist et al., 1974; Niinemets & Valladares, 2004). Models that parameterize this behavior have shown that including plant hydraulics creates vertical variation in stomatal conductance according to a balance between radiative intensity and leaf water status (e.g., Williams et al., 1996). In the multilayer canopy study by Drewry et al. (2010), the sensitivity of photosynthesis to water stress was dampened in soybean and maize canopies when leaf stomatal conductance was linked to root zone water stress via plant hydraulics, instead of linking stomatal conductance directly to soil moisture. Their results also show the nonuniform soybean canopy was more greatly impacted by water stress in the upper canopy where leaf area density peaked. While models (e.g., Community Land Model Version 5 [CLM5] and CLM-ml; Bonan et al., 2014; Kennedy et al., 2019) have begun to depart from arbitrary soil

moisture stress parameterizations in favor of parameterizations that modulate photosynthesis and evapotranspiration via plant hydraulic traits, the impacts of such an advancement on canopy carbon uptake should be carefully examined against observations at multiple time scales, as well as the differential impacts of plant hydraulic stress in big-leaf versus multilayer canopy models.

To date, the difference between multilayer and big-leaf representations of a forest canopy regarding their simulation of the response of photosynthesis to interannual climate variations, particularly when canopy architecture, microclimate, and hydraulic status vary along a vertical gradient, has not been demonstrated. Here, we evaluate modeled IAV in peak summer GPP in big-leaf and multilayer models and investigate the extent to which vertical heterogeneity resolved in a multilayer model affects the simulated GPP response to climate IAV. We further investigate whether representing vertically varying water stress within the multilayer canopy affects the direct response of photosynthesis to interannual soil moisture stress. For this analysis, we compare two versions of a multilayer model (one keeping soil moisture stress constant at each canopy layer and one that varies soil moisture stress) with similar big-leaf models at five temperate deciduous broadleaved forest (DBF) FLUXNET sites in the Northeastern United States. We focus on these forests because temperate forests are a growing carbon sink and their sensitivity to climate fluctuations may affect the future of the Northern Hemisphere land sink (Pan et al., 2011; Shiga et al., 2018). Photosynthesis is a multivariate response; thus, we use four environmental variables (temperature, humidity, radiation, and soil moisture) to represent climate IAV. The model results are interpreted with an observationally based GPP product from eddy covariance flux tower measurements, and the sensitivity of these results to diffuse light representation in the multilayer model is also examined by using diffuse light measurements from one of the flux towers. The implications for carbon-climate coupling in terrestrial forest ecosystems are discussed.

2. Data and Methods

2.1. FLUXNET Eddy Covariance Data

FLUXNET is a global network of eddy covariance towers that measure the flux of energy, water, and CO_2 between the ecosystem and atmosphere (Pastorello et al., 2017; Williams et al., 2009). We analyze data from five temperate DBF FLUXNET sites in the eastern United States with about a decade or more of data. Harvard Forest (US-Ha1; 42.54°N, 72.17°W; 1991–2012; DOI: 10.18140/FLX/1440071) is majority red oak and red maple, mixed with hemlock and white pine. The tower and canopy heights are 30 and 23 m, respectively. Morgan-Monroe State Forest (US-MMS; 39.32°N, 86.41°W; 1999–2014; DOI: 10.18140/FLX/1440083) is a secondary successional forest located across a maple-beech to oak-hickory transition zone. Its tower and canopy heights are 48 and 27 m, respectively. The Oak Openings tower is located within an oak woodland dominated by red, white and black oak, as well as red maple (US-Oho; 41.55°N, 83.84°W; 2004–2013; DOI: 10.18140/FLX/1440088), with tower and canopy heights of 32 and 24 m. University of Michigan Biological Station (US-UMB; 45.56°N, 84.71°W; 2000–2014; 10.18140/FLX/1440093) is predominantly aspen, but the footprint also contains red oak, red maple, and beech, as well as some hemlock and white pine. Its tower and canopy heights are 46 and 21 m, respectively. Finally, Willow Creek is dominated by sugar maple and basswood (US-WCr; 45.81°N, 90.08°W; 1999–2014; DOI: 10.18140/FLX/1440095) with tower and canopy heights of 48 and 24 m.

Direct meteorological measurements with gap filling are available from each tower and include air temperature and pressure, wind speed, VPD, net shortwave (SW) and longwave radiative fluxes, and precipitation flux. These measurements are used as atmospheric forcing both for the CLM simulations described below (e.g., Pastorello et al., 2017) and for the regression analysis described in section 2.3. Gap-filled daytime-partitioned GPP estimates used here are from the FLUXNET2015 data set and are hereafter referred to as "observed" GPP (Lasslop et al., 2012). Nighttime-partitioned GPP estimates are also available from the FLUXNET2015 data set, and for some site years (e.g., 1997 at US-Ha1; 2003–2004 at US-MMS) the nighttime estimate differs substantially (Figure S1 in the supporting information). However, most of the data from the nighttime-partitioned GPP are within error of the daytime-partitioned estimates based on random error in carbon flux measurements reported for FLUXNET eddy covariance towers, which is about 20% (Richardson et al., 2006; shading in Figure S1). Each site has a history of disturbances that have occurred throughout the measurement period, some of which may have affected GPP at the interannual time scale. At US-Ha1, there was an ice storm in the winter of 2008–2009 that caused some canopy damage,

including a loss of 1.5 MgC ha^{-2} of woody debris and a reduction of LAI by 1.4 m^2 m^{-2}. At US-MMS, there was a flood in June 2012 succeeded by drought in July of 2012 directly affecting July GPP, while some insect damage occurred in 2004 and following the 2012 drought (with minimal impact). At US-WCr, there was a tent caterpillar outbreak in June 2001 causing full defoliation, with leaf recovery in July 2001 and a 30% forest overstory thinning in 2013–2014. The potential impact of these disturbances on the results is discussed in section 3.2.

Because the model simulations (described in section 2.2) require atmospheric relative humidity (RH) input and only VPD data are available without gaps, VPD is converted to RH using an empirical estimate of saturation vapor pressure via Murray (1967). This calculation sometimes results in negative RH values, which are replaced by linearly interpolating between the nearest positive neighbors. Root-zone soil water content (SWC) measurements are available at all FLUXNET sites except US-Ha1. In addition to the FLUXNET2015 data described above, we also use diffuse and total photosynthetic active radiation (PAR) measurements at US-UMB to explore the role of diffuse light on carbon uptake (see section 2.4 for methodology). Diffuse and total PAR are measured by a BF2 (2004–2012) or BF5 (2013–2014) Sunshine Sensor at the US-UMB FLUXNET tower for a total period of 2004–2014, which coincides with the FLUXNET2015 data set.

2.2. Land Model Simulations

We used a suite of CLM versions (Table 1) to simulate July GPP IAV at the sites described above. In this analysis, we focus on how the differences in vertical canopy structure and water stress parameterization between big-leaf and multilayer CLM variants affect GPP. When similar parameterizations are used, the model variants use the same parameters for biogeophysical processes, and it is through these similarities that we seek to minimize intermodel parametric and structural differences arising from other factors. For example, the multilayer version of CLM (CLM-ml) was developed as an experimental branch of the CLM to test hypotheses related to a multilayer canopy representation. While some of its physics are by necessity formulated differently from the standard CLM, much of the model structure is adopted from the previous community release of CLM (Version 4.5, see section 2.2.1) and a comparison of these two model versions isolates the impact of only a few new physical parameterizations. The newest community release of CLM (CLM5) exhibits several differences compared with CLM4.5; thus, we mainly compare two configurations of CLM5 against one another (see section 2.2.3). We note that this study does not address parametric uncertainty at the individual sites or for individual species for any of the models; however, the impact of parametric uncertainty on the results is discussed in section 4. The models and simulations are described in detail below.

2.2.1. Big-Leaf Model: CLM4.5

CLM4.5 is the land surface model within the Community Earth System Model Version 1.2 (CESM1.2) (Oleson et al., 2013). CLM simulates biogeophysical and biogeochemical processes that control exchanges of energy, water, and momentum between the soil, plant canopy, and atmosphere. Vegetation is represented by plant functional types (PFTs), and the canopy in CLM4.5 is modeled as a single, bulk leaf layer, that is, a "big-leaf" canopy. The big leaf is apportioned into a sunlit fraction that absorbs direct and diffuse light and a shaded fraction that absorbs diffuse light only. The sunlit and shaded fractions are characterized by their own photosynthesis and stomatal conductance, but canopy temperature and energy fluxes are calculated using an aggregate canopy conductance. Surface layer dynamics controlling momentum, sensible heat, and latent heat fluxes are given by Monin-Obukhov Similarity Theory (MOST) (Zeng & Dickinson, 1998). Photosynthesis (for C_3 plants) is modeled using the Farquhar et al. (1980) model, and stomatal conductance is simulated by the Ball-Berry model described in Collatz et al. (1991). Water stress is simulated with a soil moisture stress parameter, β_t, which varies from 0 to 1 according to soil water matric potential and scales the minimum stomatal conductance parameter and also photosynthetic rates. Surface hydrology is represented by a variety of parameterizations simulating several fluxes (e.g., canopy interception and throughfall, evaporation, and infiltration) that contribute to the surface water balance, given by the following equation:

$$\Delta W_{canopy} + \Delta W_{surface} + \Delta W_{snow} + \Delta W_{aquifer} + \sum_{soil\ levels} \left(\Delta w_{liq} + \Delta w_{ice}\right) = \Delta t \left[q_{rain} + q_{snow} - q_{overflow} - q_{drainage} - q_{runoff} - E_{vegetation} - E_{ground}\right], \quad (1)$$

where each ΔW is the change in water storage in the canopy, at the surface, in the snowpack, in an unconfined aquifer underneath the soil layers, respectively; while each Δw is the change in soil liquid and solid

Table 1
Model Configuration Descriptions for Each Simulation

Simulation	Canopy type	Soil moisture	Stomatal conductance	Water stress type	Reference for model
CLM4.5	Big leaf	Simulated and coupled with canopy	Ball-Berry (Collatz et al., 1991)	Soil moisture stress factor, β_t	Oleson et al. (2013)
CLM-ml-BB	Multilayer	Prescribed from CLM4.5 run	Ball-Berry (Collatz et al., 1991)	Soil moisture stress factor, β_t	Bonan et al. (2014, 2018)
CLM-ml-SPA	Multilayer	Prescribed from CLM4.5 run	Water use efficiency (Bonan et al., 2014; Williams et al., 1996)	Plant hydraulic stress via minimum leaf water potential threshold, $\psi_{l,min}$ (Bonan et al., 2014; Williams et al., 1996)	Bonan et al. (2014, 2018)
CLM5-PHS	Big leaf	Simulated and coupled with canopy	Medlyn (Medlyn et al., 2011)	Plant hydraulic stress via water potential threshold for 50% xylem conductivity, P_{50}, embedded in water stress factor, f_w (Kennedy et al., 2019)	Lawrence et al. (2019)
CLM5-noPHS	Big leaf	Simulated and coupled with canopy	Ball-Berry (Collatz et al., 1991)	Soil moisture stress factor, β_t	Lawrence et al. (2019)

water content at each soil layer, summed over soil layers. The change in total water storage during each time step, Δt, depends on the strength of liquid water and evaporative fluxes represented by q and E, respectively. A detailed description of the individual parameterizations for each hydrological process is provided in Oleson et al. (2013).

CLM4.5 simulations are run in off-line, "single-point" mode to simulate the fluxes at an eddy covariance flux tower and use meteorological observations from the tower as atmospheric boundary conditions. Simulations are run for the years of data available at each site. A representative PFT is used for each site (in this case DBF at all sites), and only the canopy and soil biogeophysical processes are simulated in response to the atmospheric forcing. Phenology, or the seasonal evolution in LAI, is derived from satellite data and is prescribed as a climatological monthly mean without IAV (Lawrence & Chase, 2007). The default biogeophysical parameters for DBF are used (Oleson et al., 2013), and ambient CO_2 is held constant at 360 ppm. All CLM4.5 simulations are initialized from the same "arbitrary initial conditions," which are preselected in the CLM code (Oleson et al., 2013, pp. 27). For the land surface, this means that moisture is initialized at 0.15 $m^3\ m^{-3}$ and soil temperature at 274 K throughout the soil column, while vegetation temperature is initialized at 283 K. These simulations provide a standard big-leaf baseline for simulation of the response of GPP to climate and also simulated soil moisture for prescription in CLM-ml (see section 2.2.2).

2.2.2. Multilayer Model: CLM-Ml

We use a multilayer version of CLM (CLM-ml) to test the impacts of resolving the vertically structured canopy microenvironment on the IAV of carbon uptake in forests (Bonan et al., 2014, 2018). CLM-ml models the canopy as a stack of thin (0.5 m) big-leaf layers, each divided into sunlit and shaded fractions with unique leaf-level characteristics (e.g., leaf temperature and stomatal conductance). LAI varies with height according to a beta distribution function (dLAI in Figure 1e) for a typical DBF canopy, which we refer to as a nonuniform distribution throughout the paper. Each bulk leaf layer is associated with and exchanges fluxes with an individual atmospheric layer, which in turn communicates with each neighboring atmospheric layer. Scalar profiles (wind speed, temperature, and vapor pressure) are computed using a set of coupled flux-profile equations that account for canopy-induced turbulence above and within the canopy (Bonan et al., 2018).

CLM-ml has two representations for photosynthesis-stomatal conductance coupling and water stress: (1) a conventional, empirical model (Ball-Berry, β_t; same as CLM4.5 but with β_t applied equally at all leaf layers) and the (2) the soil-plant-atmosphere model (SPA; Williams et al., 1996, 2001). When the water potential in vegetation leaves, and by consequence in the stem, drops due to water stress, cavitation (i.e., dissolution of air and bubble formation) occurs and can lead to embolism (i.e., complete blockage to flow). Trees prevent this by closing their stomates before the negative pressure grows intense enough to cause cavitation and loss of hydraulic conductance (Tyree & Ewers, 1991). This process is referred to here as plant hydraulic stress. Plant hydraulics in SPA are represented by two PFT-specific parameters, stem hydraulic conductance, and stem hydraulic capacitance, which moderate leaf water potential (LWP) in each layer depending on soil water potential, leaf layer transpiration rate, and hydraulic head (i.e., gravitational potential). Stem

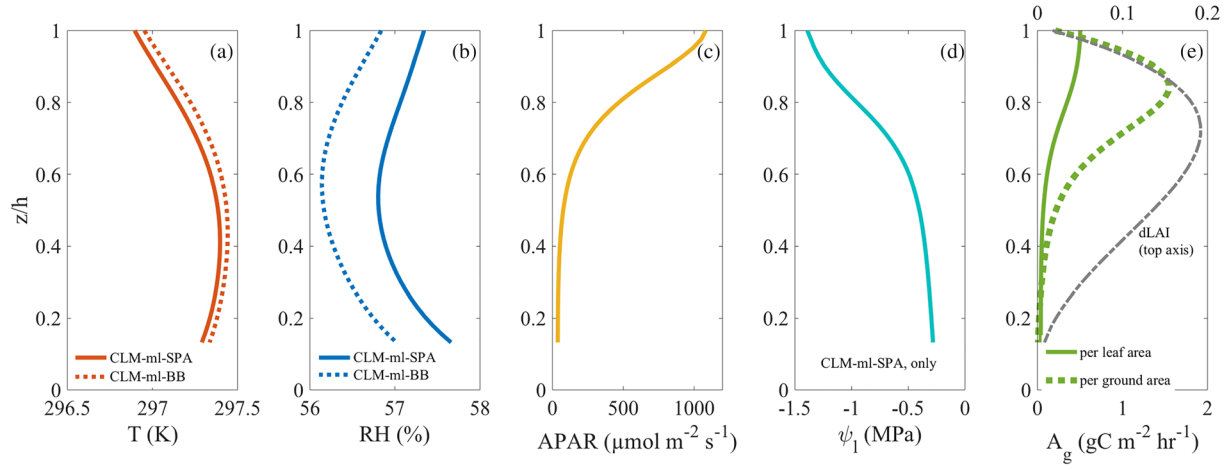

Figure 1. Mean daytime vertical profiles in CLM-ml (US-UMB) (averaged over 10 a.m. to 4 p.m. over 2001–2014) for (a) air temperature (T), (b) relative humidity (RH), (c) absorbed photosynthetic active radiation (APAR), (d) leaf water potential (LWP, here ψ_l), and (e) gross carbon assimilation rate (a_g) and leaf area density (dLAI) distribution (top axis). z/h is relative height within canopy of height h.

hydraulic conductance determines the rate of xylem flow, which transports water from soil to leaf through the bole and branches of the tree, while stem hydraulic capacitance determines the amount of water retention in the xylem. Stomatal conductance is calculated to optimize water use efficiency (a PFT-specific constant), subject to the constraint that LWP exceeds a defined minimum, also a PFT-specific constant (Bonan et al., 2014). Doing so alters the coupling between stomatal conductance and soil moisture by adding a plant hydraulic mechanism between soil water and water stress in the leaf layer, which is linked to LWP instead of directly to soil moisture.

Two configurations of the multilayer model are used in this study to parse the effects of the alternative stomatal conductance and plant hydraulics representations. The first version, CLM-ml-BB, is comparable to CLM4.5 as it uses Ball-Berry stomatal conductance and the soil moisture stress (β_t) is applied equally to all leaf layers, though it uses the different turbulence and energy closure methods mentioned above. The second version, CLM-ml-SPA, uses the SPA model wherein soil moisture stress varies vertically because plant hydraulics modulate between soil water potential and LWP at each leaf layer. While both configurations of the model include the multilayer resolution of canopy physics, the effects of vertically varying water stress are unique to CLM-ml-SPA. The plant hydraulics in CLM-ml-SPA may change the susceptibility of photosynthesis to canopy microclimate by linking water stress to within-canopy microclimate, that is, by applying plant hydraulic stress (i.e., closure of stomata) to leaves that have lost moisture by radiation-transpiration coupling.

Because CLM-ml is currently an off-line model formulation, it is not fully coupled to all CLM processes. In the simulations presented here, CLM-ml SWC is decoupled from precipitation and evapotranspiration, requiring prescribed soil moisture input and limiting simulations to shorter (approximately monthly) time scales. CLM-ml simulations are therefore run with volumetric SWC and β_t prescribed from the CLM4.5 simulations described in section 2.2.1 and are run for the month of July (peak growing season), only. These simulations are run in off-line, single-point mode for the same years as the CLM4.5 simulations and are driven by the same FLUXNET atmospheric forcing, also with constant CO_2 (360 ppm). The results of these simulations, along with the CLM4.5 simulations, are discussed in sections 3.1–3.3.

2.2.3. CLM5 and Big-Leaf Plant Hydraulics

The most recent implementation of CLM is Version 5 (CLM5), which includes new hydrology, plant hydraulic stress (PHS), and the Medlyn stomatal conductance scheme (Kennedy et al., 2019; Medlyn et al., 2011). The model, similar to SPA, links stomatal conductance to plant water stress by mediating SWC and transpiration via a plant hydraulics scheme that maintains continuity of water mass throughout the soil-plant-atmosphere system, except that the canopy is modeled by a big-leaf representation that is divided into sun and shaded portions, similar to CLM4.5. There are several distinctions to note between CLM5 PHS and the CLM-ml-SPA model that do not allow direct comparisons of their implementation of plant hydraulic

stress (in addition to the differing canopy physics). For one, plant hydraulic status (i.e., LWP in the models) is linked directly to stomatal closure in SPA, while in CLM5 PHS a *plant* water stress parameter (f_w) is calculated as a sigmoidal function parameterized by threshold LWP corresponding to 50% hydraulic conductance and applied in the Medlyn equation for stomatal conductance (similar to β_t in CLM4.5). Second, SPA includes hydraulic capacitance, which represents water storage in the plant hydraulic system, while CLM5 PHS does not. Third, the iterative process by which stomatal conductance is calculated differs between SPA and CLM5.

Despite these differences, we can infer whether plant hydraulics affect GPP in a big-leaf representation by comparing two configurations of CLM5 with different settings: (i) PHS turned *on* (CLM5-PHS) and (ii) PHS turned *off* (CLM5-noPHS). When CLM5 is run with PHS turned off, the stomatal conductance parameterization is Ball-Berry and water stress is implemented as in CLM4.5 with a soil moisture stress factor, β_t, which comes directly from the SWC as opposed to the plant water stress parameter f_w used with PHS turned on. We note that even though these simulations also differ in stomatal conductance parameterization (Medlyn vs. Ball-Berry), additional simulations (not shown) showed that the choice of stomatal conductance parameterization had a small impact on simulated July GPP compared to turning plant hydraulics on and off. Simulations of CLM5 using each of the two configurations are run at each FLUXNET site similar to the CLM4.5 and CLM-ml runs described above, and the resulting IAV in GPP simulated by these model runs is analyzed with respect to the observations and other models. The CLM5 results are discussed in section 3.5.

2.3. Analysis of IAV

We analyze IAV in the month of July, which represents peak growing season and identifies GPP responses to the direct effects of local climate variability. Although the FLUXNET observations of July GPP IAV might reflect lagged responses to climate IAV earlier in the growing season because of phenological responses to climate (Desai, 2010), the model as described above has a fixed phenological cycle and will only reflect lagged responses of GPP via lagged responses of soil moisture to prior months' climate. Otherwise, the model is representing GPP responses to July climate variability only. IAV is defined here as the annual anomaly of July GPP from the mean of July GPP over all simulated years. We define the magnitude of July IAV as the standard deviation of the July anomalies from the long-term trend (S_{IAV}),

$$S_{IAV} = \frac{\sqrt{\sum_{i=1}^{N}\left(y_i - y_{i,\,fit}\right)^2}}{N-1}. \tag{2}$$

Here, y_i is the annual July value (mean or sum) for year i, and $y_{i,fit}$ is simple linear best fit of annual July values over a time series of N years. Annual July values for GPP and leaf layer gross carbon assimilation rate (a_g) are the sum of hourly carbon uptake over the month of July. For all observed climatic driving variables (air temperature; RH, and incoming SW radiation, as well as SWC [i.e., soil moisture]) simulated by CLM4.5, y_i is the July mean only including timestamps when GPP > 0. In addition to soil moisture, which for CLM4.5 and CLM-ml is simulated by CLM4.5 and also simulated in CLM5, IAV in observed precipitation accumulated from March–July (which correlates well with simulated SWC, Table 2) is calculated for additional insight.

The year-to-year pattern of variability is quantified as the sample z score of the detrended anomalies:

$$y_{IAV} = \frac{y_i - y_{i,\,fit}}{S_{IAV}} \times 100 \tag{3}$$

where y_{IAV} is the annual July anomaly relative to S_{IAV} in units of percent. A z score of 100% indicates a positive anomaly equal to one standard deviation from the mean. Using a z score allows the patterns of IAV in carbon flux and driving climate variables to be represented as anomalies relative to the *magnitude of variability* (i.e., S_{IAV}) and thus for variables to be compared directly, independent of their units or magnitude. Note that, because the data for one or another variable may not be normally distributed, the z score as utilized here is *not* representative of how close a data point is to the most likely values. To determine the response of GPP to climate IAV, a simple linear regression analysis is performed by regressing y_{IAV} of whole-canopy GPP (CLM4.5, CLM-ml, and observations) with y_{IAV} of climatic drivers as

Journal of Geophysical Research: Biogeosciences
10.1029/2020JG005658

Table 2
Coefficient of Correlation for Canopy-Scale Linear Regressions of z_{IAV}

Site	Variable	T	RH	SW	Pr	SWC[a]	GPP, obs
US-Ha1	RH	−0.17					
	Incoming SW	0.20	−0.76***				
	MAMJJ Accum. Precip.	−0.39*	0.03	0.05			
	SWC	−0.41*	0.14	−0.04	0.84***		
	GPP, obs	0.44**	−0.34	0.51**	0.15	N/A	
	GPP, CLM4.5	0.32	−0.36**	0.46*	−0.39*	−0.49**	0.27
	GPP, CLM-ml-BB	0.40*	−0.28	0.41*	−0.39*	−0.50**	0.33
	GPP, CLM-ml-SPA	0.11	−0.47**	0.57***	−0.23	−0.37*	0.26
	GPP, CLM5-PHS	0.15	−0.36	0.48**	−0.40*	−0.49**	0.18
	GPP, CLM5-noPHS	0.16	−0.35	0.49**	−0.42*	−0.55***	0.20
US-MMS	RH	−0.44*					
	Incoming SW	0.37	−0.59*				
	MAMJJ Accum. Precip.	−0.15	0.20	0.06			
	SWC	−0.68**	0.56*	−0.36	0.62		
	GPP, obs	−0.52**	0.39	0.13	0.37	0.67***	
	GPP, CLM4.5	−0.59**	0.72**	−0.12	0.44*	0.77***	0.87***
	GPP, CLM-ml-BB	−0.59**	0.72**	−0.12	0.45*	0.77***	0.87***
	GPP, CLM-ml-SPA	−0.57**	0.58**	0.06	0.26	0.54**	0.81***
	GPP, CLM5-PHS	−0.70***	0.70***	−0.09	0.47*	0.80***	0.79***
	GPP, CLM5- noPHS	−0.63**	0.69***	−0.05	0.47*	0.83***	0.82***
US-Oho	RH	−0.21					
	Incoming SW	0.32	−0.91***				
	MAMJJ Accum. Precip.	−0.27	0.47	−0.41			
	SWC	−0.30	0.73**	−0.65*	0.58		
	GPP, obs	−0.59*	−0.39	0.09	0.03	−0.10	
	GPP, CLM4.5	−0.49	0.74**	−0.67**	0.72**	0.94***	−0.01
	GPP, CLM-ml-BB	−0.47	0.75**	−0.68**	0.74**	0.94***	−0.02
	GPP, CLM-ml-SPA	−0.89***	0.25	−0.26	0.36	0.52	0.46
	GPP, CLM5-PHS	−0.86**	−0.04	−0.06	0.37	0.34	0.36
	GPP, CLM5- noPHS	−0.75*	0.06	−0.03	0.21	0.49	0.15

Journal of Geophysical Research: Biogeosciences
10.1029/2020JG005658

Table 2
Continued

Site	Variable	T	RH	SW	Pr	SWC[a]	GPP, obs
US-UMB	RH	−0.48*					
	Incoming SW	0.68***	−0.74***				
	MAMJJ Accum. Precip.	0.26	0.46**	−0.07			
	SWC	−0.07	0.46	−0.16	0.82***		
	GPP, obs	−0.02	0.23	0.12	0.22	0.33	
	GPP, CLM4.5	−0.11	0.52*	−0.21	0.86***	0.82**	0.25
	GPP, CLM-ml-BB	−0.10	0.52*	−0.20	0.87***	0.82**	0.26
	GPP, CLM-ml-SPA	0.18	0.34	0.09	0.70***	0.43	0.25
	GPP, CLM5-PHS	0.32	0.49	−0.10	0.89***	0.80***	0.05
	GPP, CLM5- noPHS	−0.39	0.63**	−0.43	0.75***	0.73***	0.11
US-WCr	RH	0.26					
	Incoming SW	0.65**	0.43				
	MAMJJ Accum. Precip.	0.25	−0.04	0.56**			
	SWC	0.21	0.36	0.67***	0.74***		
	GPP, obs	−0.64**	0.40	−0.17	−0.04	−0.03	
	GPP, CLM4.5	0.33	0.25	0.68***	0.74***	0.86***	0.61**
	GPP, CLM-ml-BB	0.30	0.28	0.69***	0.75***	0.89***	0.64*
	GPP, CLM-ml-SPA	0.46*	0.31	0.44	0.47	0.56**	0.54**
	GPP, CLM5-PHS	0.17	−0.05	0.20	0.45	0.47*	0.50
	GPP, CLM5- noPHS	−0.26	−0.13	0.17	0.46	0.54	0.35

Note. Green shaded cells are covariances of drivers, while blue shaded cells are correlations of GPP with drivers. White numerical cells in the rightmost column are correlations of modeled GPP with observed GPP.
[a]Observed GPP was regressed with observed SWC. CLM4.5 and CLM-ml GPP were regressed with CLM4.5-simulated SWC. CLM5-PHS and CLM5-noPHS were simulated with their own respective simulated SWC $^{*}p < 0.10$. $^{**}p < 0.05$. $^{***}p < 0.01$.

independent variables. Regressions are also performed between a_g at individual leaf layers (CLM-ml, only) and climatic drivers to determine if there is a vertically varied response of carbon uptake to interannual climate variability. Finally, all of the climatic variables are regressed with one another to determine the linear covariance between drivers. Stepwise multiple linear regressions were also calculated for GPP and a_g IAV using the four drivers as possible independent variables (not shown); however, the results for the multiple linear regression analysis (i.e., the significant drivers it identified) were similar to the simple linear regression, so we show the simple linear regression only for clarity.

In CLM-ml, the top of the canopy is represented by a height, h. Therefore, all multilayer results displayed as a function of height are presented using relative height within the canopy, or z/h, where height varies from 0 (ground) to 1 (canopy top, h).

2.4. Simulating Diffuse Light Effects on GPP in CLM-Ml

We additionally evaluate the partitioning of diffuse versus direct light in CLM to determine whether canopy complexity influences the sensitivity of carbon uptake to radiation. The radiation scheme in off-line CLM equally partitions SW radiation into visible and near-infrared energy. The visible and near-infrared bands are further partitioned into direct and diffuse light using an empirical polynomial fit to the climatological diurnal cycle of surface-level radiation simulated by the Community Atmosphere Model Version 3 (Oleson et al., 2013). In this parameterization, diffuse fraction always decreases as total visible light intensity increases, while diffuse light intensity is nonlinearly related to visible intensity (Figure S2). We perform additional linear regressions of gross carbon assimilation in each leaf layer (CLM-ml, only) with direct and diffuse visible intensity.

Because the direct-diffuse partitioning parameterization is based on climatology, we test the sensitivity of the multilayer model regressions to this parameterization by running simulations with diffuse fraction prescribed from the available hourly PAR measurements at US-UMB from 2004 to 2014. Observed diffuse fraction behaves differently as a function of total radiation compared to the climatological CLM parameterization. Instead of early decline of diffuse fraction at low SW irradiance like in the parameterization, observed diffuse fraction remains high at lower irradiance and begins to steeply fall off at higher SW intensities (Figure S3). Moreover, observed diffuse fraction depends on zenith angle (i.e., time of day) and also exhibits substantial variability aside from its relationship to solar intensity and zenith angle, likely due to changes in clouds and aerosols. The observed diffuse fraction tends to be higher than that of the parameterization and is partly decoupled from total visible intensity. To verify whether the diffuse fraction parameterization affected the simulated carbon uptake, we analyze an additional simulation using the prescribed diffuse fraction. Because diffuse fraction data are only available from 2004–2014, we repeat the regressions of the simulations with parameterized diffuse fraction for model output from 2004–2014 only for consistency.

3. Results

3.1. Canopy Vertical Structure in CLM-Ml

Vertical structure in CLM-ml manifests in vertically varying environmental conditions, of which radiation primarily controls the average daytime profile of carbon assimilation rate, together with leaf area density (Figure 1). At US-UMB, temperature and RH nonmonotonically vary throughout the canopy, where temperature has a maximum and RH, a minimum in the middle of the canopy (Figures 1a and 1b). The exact position of these maxima varies in shorter or taller canopies, but these profiles are similar for all sites based on the same leaf area distribution. CLM-ml-BB is warmer and drier than CLM-ml-SPA throughout the canopy, although vertical variations in temperature and RH are small at all sites (T within 0.5 K and RH within 0.85%). Light is extinguished exponentially from the topmost layers to the bottom (Figure 1c) in both model versions. LWP, only modeled in CLM-ml-SPA, is depleted in the upper canopy where the rate of photosynthesis is highest and therefore stomata are most open, coinciding with high VPD driven by high direct insolation. Water stress is mostly limited to $z/h > 0.6$, since below this level, leaves are more shaded, and LWP is maintained at roughly −0.5 MPa (Figure 1d). The profile of gross carbon assimilation rate per leaf area (Figure 1e, solid line) is primarily controlled by absorbed photosynthetic active radiation (APAR), and it follows the same exponential decline from top to bottom of canopy. However, when the leaf area density distribution is taken into account (Figure 1e, dashed line), gross carbon assimilation rate

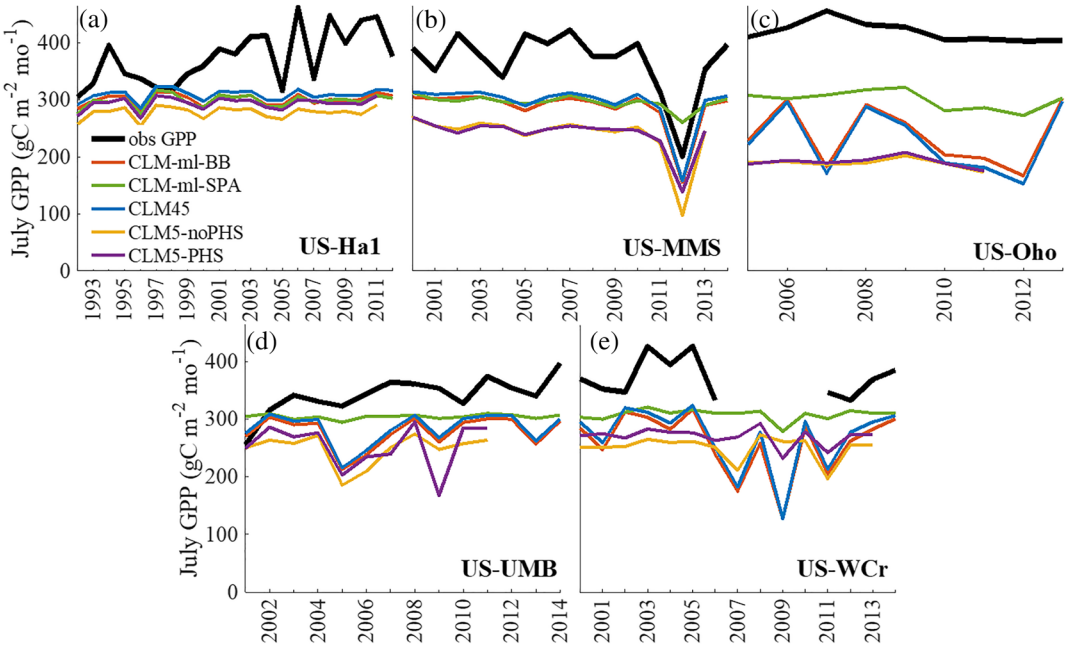

Figure 2. Time series of mean July GPP for the FLUXNET daytime-partitioned estimate and various configurations of CLM models (see Table 1) for sites (a) US-Ha1, (b) US-MMS, (c) US-Oho, (d) US-UMB, and (e) US-WCr. The US-WCr site is missing data from years 2007–2010.

increases to a maximum near $z/h = 0.8$ and then decreases exponentially to the canopy bottom. Integrated canopy GPP relies on this gross carbon assimilation rate adjusted for leaf area density and indicates that the maximum contribution in the canopy to GPP is from the upper midcanopy.

3.2. Canopy-Scale IAV of GPP and Its Response to Climate Variability

The response of observed July GPP to climate variability at each site generally depends on the climatic driver(s) with the most pronounced IAV (Tables 2 and S1). US-Ha1 is the most humid and cool of all the sites and receives the least insolation on average. Despite low average values, incoming SW radiation is characterized by larger IAV than other driver variables at the site, and GPP IAV at US-Ha1 is most highly correlated with SW radiation ($r = 0.51$; Table 2). These regressions at US-Ha1 are robust even when the years of notable disturbance (see section 2.1) are removed (Table S2). US-MMS is the warmest site, receives the most precipitation, and also has the highest temperature and precipitation IAV. US-MMS has the highest IAV of observed July GPP ($S_{IAV} = 55.54$ gC m^{-2} month^{-1}; Table S1), and this is most highly correlated with IAV in soil moisture ($r = 0.65$; Table 2), which is mediated by evaporative demand and precipitation. GPP IAV at US-MMS is anticorrelated with temperature ($r = -0.52$; Table 2), and we note that temperature is anticorrelated with soil moisture. We note that 2012 was a drought year at US-MMS characterized by very low RH and soil moisture, which is a strong driver of the correlations at US-MMS. The linear correlation of GPP with soil moisture is substantially weakened ($r = 0.29$; $p > 0.10$) when the year 2012 is removed from the analysis, as is the correlation of GPP with temperature ($r = -0.21$; $p > 0.10$) while the only significant correlation ($p < 0.01$) becomes that of observed GPP and RH (Table S2). This suggests that outside of a drought at a relatively well watered site like US-MMS, GPP may be far more responsive to atmospheric conditions than soil conditions. GPP at US-Oho is the highest in magnitude, which may be due to this site having the highest SW radiation but lowest in IAV. Like US-MMS, GPP at US-Oho is anticorrelated with temperature. US-UMB exhibits the lowest climate variability of all of the sites, which may account for the lack of strong ($|r| > 0.5$) or significant ($p < 0.05$) correlations between GPP IAV and any of the observed climate drivers given by the linear regressions (Table 2). Finally, at US-WCr, GPP is anticorrelated with temperature, while temperature at US-WCr has the second highest IAV among the sites. RH becomes a significant driver at US-WCr, as well, when accounting for disturbance history (Table S2); otherwise, the regressions remain qualitatively similar.

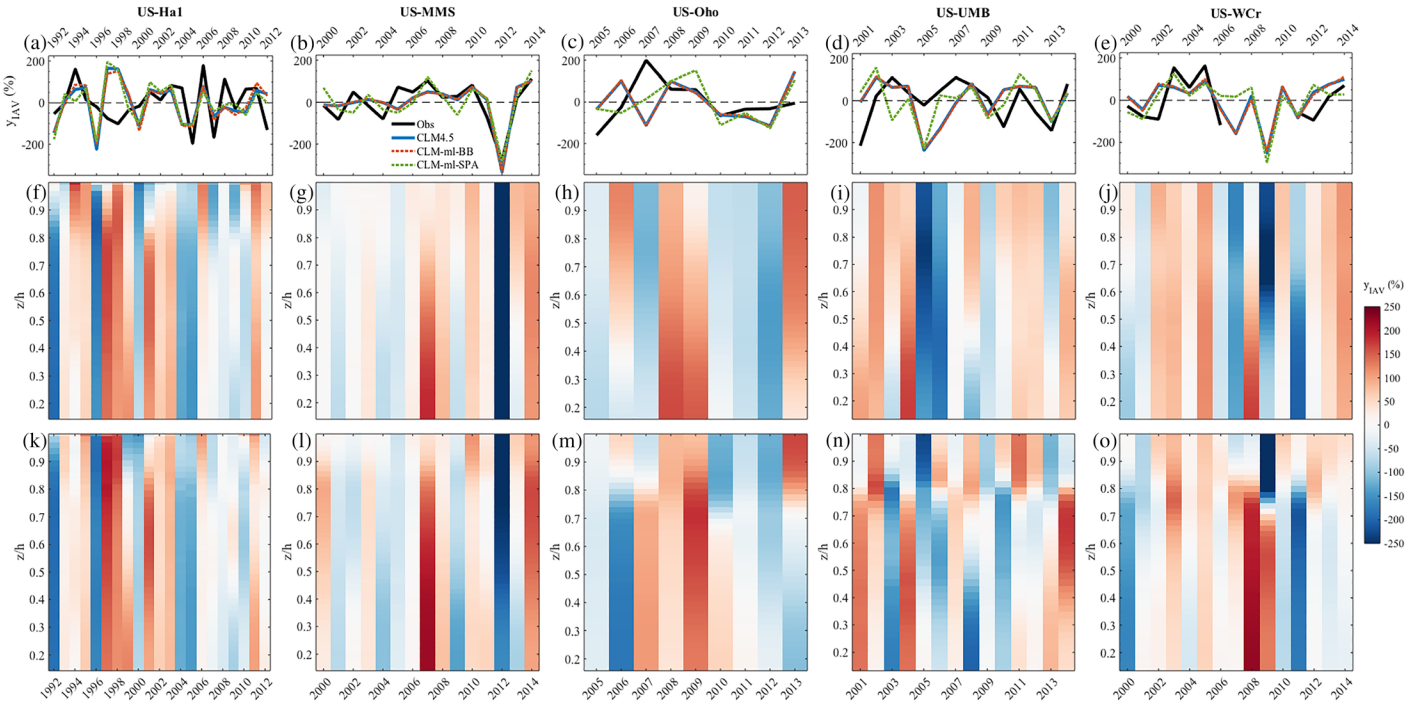

Figure 3. y_{IAV} for (a–e) GPP at the canopy scale, (f–j) carbon assimilation rate at each leaf layer in CLM-ml-BB, and (k–o) carbon assimilation rate at each leaf layer in CLM-ml-SPA. Note the different years for each site. z/h is relative height within canopy of height h.

The models consistently underestimate observed July GPP at all sites by 11–46% (Figure 2 and Table S1), which may be due to either parameter or model structural uncertainty (see section 4). The simulations do, however, capture some of the observed patterns of GPP (Table 2). For example, the models capture the positive correlations of GPP with incoming SW radiation and temperature and negative correlation with RH at US-Ha1. They also capture the anticorrelation of GPP with temperature at US-Oho. However, some of that agreement diminishes when disturbance years are removed from the analysis, like at US-Ha1 (Table S2). Model-observation agreement on the whole is fairly weak, disturbances or not, as correlations of observed GPP with SWC are weak while the models still simulate a strong sensitivity of simulated GPP to SWC. Therefore, the modeled GPP IAV does not correlate well with observed GPP IAV at any of these sites. These results suggest that either the models overemphasize the role of soil moisture variability in GPP IAV or that there are errors between CLM4.5 simulated SWC and real-world soil moisture.

Differences between GPP IAV simulated by CLM-ml-BB and CLM4.5 and their regressions with climatic drivers are negligible for all sites (Tables 2 and S1 and Figure S4), implying that vertically varying microclimate and leaf area profile did not substantially impact the response of GPP to climate IAV. However, the results are notably different when using SPA, indicating that simulating plant hydraulics and LWP in a multilayer model may influence the IAV of GPP. CLM-ml-SPA simulations dampen July GPP IAV relative to CLM-ml-BB and CLM4.5 at all sites except US-Ha1 (Table S1 and Figures S4a–S4d). At US-Ha1, simulated July GPP IAV at was slightly greater in CLM-ml-SPA than it was for CLM4.5 and CLM-ml-BB (Table S1). Moreover, at all sites except US-Ha1, SPA alters the pattern of GPP IAV relative to the Ball-Berry simulations, causing y_{IAV} for some years to differ by over 100% between simulations (Figures 3b–3e). At US-Ha1, the pattern of CLM-ml-SPA simulated July GPP IAV changes little relative to that of CLM-ml-BB and CLM4.5 (Figure 3a). To explain why the multilayer model only made a difference when using SPA, we analyze the individual leaf layers simulated in CLM-ml in section 3.3.

3.3. IAV of Gross Carbon Uptake and Response to Climate Variability in Individual Leaf Layers

In the multilayer model simulations, IAV of gross carbon assimilation rate (a_g) differs among individual leaf layers (Figures 3f–3o), indicating that each layer can respond independently to climate IAV. This is most apparent in the CLM-ml-SPA simulations, where vertical gradients in a_g IAV are very strong. Moreover,

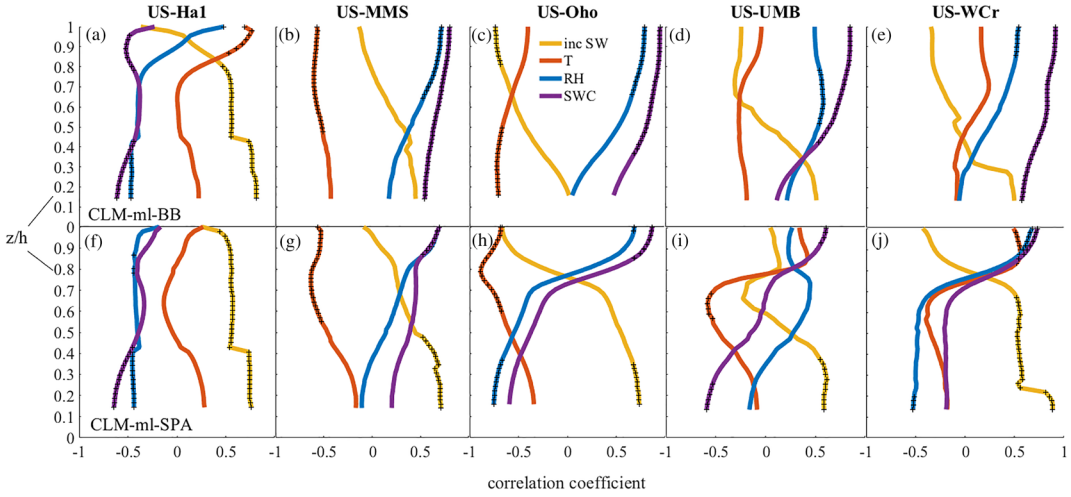

Figure 4. Correlation coefficients between y_{IAV} of carbon assimilation rate at each leaf layer and y_{IAV} of the climate drivers in CLM-ml-BB (a–e) and CLM-ml-SPA (f–j). Stippled (+) points represent $p < 0.05$. z/h is relative height within canopy of height h.

at some layers the sign may be opposite to that of other layers and even the canopy integrated GPP (Figures 3a–3e), indicating that the climate-driven anomalies at some layers oppose the anomalies at other layers in the same year. In fact, these vertical gradients are explained by a vertically varying response to climate variability (i.e., different dominant drivers at each layer), as measured by the correlations between y_{IAV} of gross carbon assimilation rate (a_g) at individual canopy layers with the y_{IAV} of four climate drivers (Figure 4). To elucidate how either multilayer parameterization, CLM-ml-BB or CLM-ml-SPA, affects these results, we analyze Figures 3 and 4 in the context of each simulation across all five sites.

In the CLM-ml-BB simulations, vertical gradients in a_g IAV are most apparent at US-Ha1 within the upper part of the canopy (Figure 3f), with vertical gradients present at all sites we simulated (Figures 3g–3j). For CLM-ml-BB simulations, the sign of the a_g anomaly at each layer is fairly uniform throughout the canopy, with some exceptions where there are sign changes in the mid and lower canopy (e.g., 2003 and 2008 at US-UMB, Figure 3i; 2000 at US-WCr, Figure 3j). For most years, the sign of the anomaly in each canopy layer corresponds to the sign of the integrated GPP IAV time series for CLM-ml-BB in Figures 3a–3e. At all sites except US-Ha1, soil moisture was the main limiting climate variable throughout the canopy, shown by the significant ($p < 0.05$), positive correlation coefficients in the linear regressions at most layers (Figures 4b–4e). This relatively consistent soil moisture response throughout the canopy explains why GPP IAV is so similar between CLM-ml-BB and CLM4.5. The sign of the correlations changes within the canopy in the CLM-ml-BB simulations at some sites (excluding US-Ha1) because of the increasing dependence of a_g on radiation, in tandem with incoming SW radiation anomalies that have the opposite impact on a_g of soil moisture. For example, in years 2003 and 2008 at US-UMB (Figure 3i), negative radiation anomalies (Figure S4d) drove negative a_g anomalies at $z/h < 0.4$, while positive SWC anomalies drove positive a_g anomalies at $z/h > 0.4$, resulting in positive anomalies in canopy-integrated GPP. Of the five deciduous sites evaluated, US-Ha1 exhibits different behavior with CLM-ml-BB and is mainly limited by radiation (Figure 4a). The transition from temperature-limited carbon uptake to radiation-limited carbon uptake at around $z/h \sim 0.84$ caused strong vertical variation in leaf layer a_g IAV near that height (Figure 3f). However, radiation was still the main driver throughout the canopy, which accounts for the similarities between CLM-ml-BB and CLM4.5 simulations at this site.

Other climatic drivers that have significant correlations in the CLM-ml-BB simulations can be explained via their covariation with the main driving climate variable (SWC or radiation) at any site. The negative trends of carbon uptake with SWC and RH at US-Ha1 (Figure 4a) likely stem from their opposing relationship with radiation (Figure 2a). Temperature is significantly negatively correlated with carbon uptake at US-MMS in $z/h > 0.45$ (Figure 4b), but this may arise from an anticorrelation between temperature and SWC at US-MMS

(Table 2). Likewise, at US-Oho radiation is strongly anticorrelated, and temperature weakly anticorrelated, with SWC and RH.

In contrast, the CLM-ml-SPA simulations show stronger vertical gradients, and there are frequently sign changes within the canopy, especially at US-UMB. The vertically varying water stress in CLM-ml-SPA is predominantly why it produces qualitatively and quantitatively different regression coefficients at each layer compared to those from CLM-ml-BB, mainly at soil moisture-limited sites (Figures 4g–4j). In CLM-ml-SPA, soil moisture dependence is limited to the uppermost leaf layers, which results in other climatic variables driving IAV in photosynthesis lower in the canopy. At US-MMS, US-UMB, and US-Oho, there are three different regimes of photosynthetic response to climate variability: The upper canopy is mainly limited by soil moisture, the middle, by temperature, and the lower, by radiation (Figures 4g–4i). At US-WCr, there are only two vertical regimes—one driven by a combination of SWC, RH and temperature at the top, and one dominated by radiation at the bottom (Figure 4j). Different drivers at different layers result in the transitions between positive and negative IAV among the leaf layers (Figures 3l–3o). This occurs because since some years have anomalies in one climatic driver that oppositely affect carbon uptake compared to the effect of another climatic driver. A clear example is at US-UMB in year 2011, when high radiation and relatively higher SWC caused positive anomalies at the top and bottom of canopy, while high temperature caused a negative anomaly in the middle of the canopy (Figures 3n and 2d). Many of the site years characterized by sign changes within the canopy were associated with damped GPP IAV in CLM-ml-SPA relative to CLM-ml-BB, as is evident, for example, at US-Oho in 2006 and 2007 (Figures 3c and 3m), or at US-UMB in 2004 and 2006 (Figures 3d and 3n). In fact, damped response to soil moisture can also explain why CLM-ml-SPA would predict in one year a canopy-integrated GPP anomaly of opposite sign to that predicted by CLM-ml-BB. For example, at US-UMB in 2003, a year with positive soil moisture anomaly and negative radiation and humidity anomalies (Figure S4d), CLM-ml-BB predicted a positive anomaly in GPP due mainly to positive a_g anomalies in the upper two thirds of the canopy while CLM-ml-SPA predicted a negative GPP anomaly mainly due to the lower three quarters of the canopy (Figure 3d). In this example, CLM-ml-BB was responding to the positive soil moisture anomaly, while CLM-ml-SPA with a damped soil moisture dependence was responding more to the negative radiation and humidity anomalies. In contrast to soil moisture-limited sites, at US-Ha1 where radiation was the dominant driver, the layer-by-layer correlations are similar to those of the CLM-ml-BB simulation (Figure 4f), and the patterns of IAV in the multilayer canopy are also similar (Figures 3f and 3k), further suggesting that SPA has a stronger impact on GPP at soil moisture limited sites.

3.4. Diffuse Light Effect on GPP

The results presented in section 3.3 suggest that multilayer canopy structure may affect the response of GPP IAV to climate variability when plant hydraulic stress is vertically resolved, exposing radiation limitation in the lower part of the canopy that was overshadowed by soil moisture limitation in traditional schemes (Figures 4f–4j). We therefore test whether the GPP IAV is sensitive to the diffuse parameterization used in the model because these lower canopy layers receive mostly diffuse light. Previous studies have shown that increased diffuse light fraction increases GPP (Gu et al., 2002; Niyogi, 2004), although other studies suggest that this effect is weak in forests (Cheng et al., 2015). Simulations using prescribed diffuse fraction from measured PAR at US-UMB reveal that variations in radiation were an important driver of GPP IAV at $z/h = 0.6$–0.8 (Figure 5c), whereas the radiation trends at these leaf layers were not significant when diffuse fraction was parameterized (Figure 5a). Diffuse evaluations at other sites were not possible due to the lack of historical diffuse radiation measurements.

Regressions with the direct and diffuse components of the visible spectrum show that the increased dependence of a_g on diffuse radiation in the middle layers of the canopy is cause for the increased dependence on total SW radiation. Diffuse light positively drives a_g in the midcanopy in simulations with prescribed diffuse fraction, and conversely, direct visible light has a negative impact on a_g, likely because it increases temperature and VPD which have a negative impact on photosynthesis.

July GPP magnitude increased for all years with prescribed diffuse fraction relative to simulations with parameterized diffuse fraction (Figure 6a). The prescribed diffuse shows some cases where it influences IAV, for example, the large decrease in IAV from 2004–2006 (Figure 6a), but overall, the impact on GPP IAV does not improve agreement with observations (Figure 6b). On hourly time scales of the light response curves, the

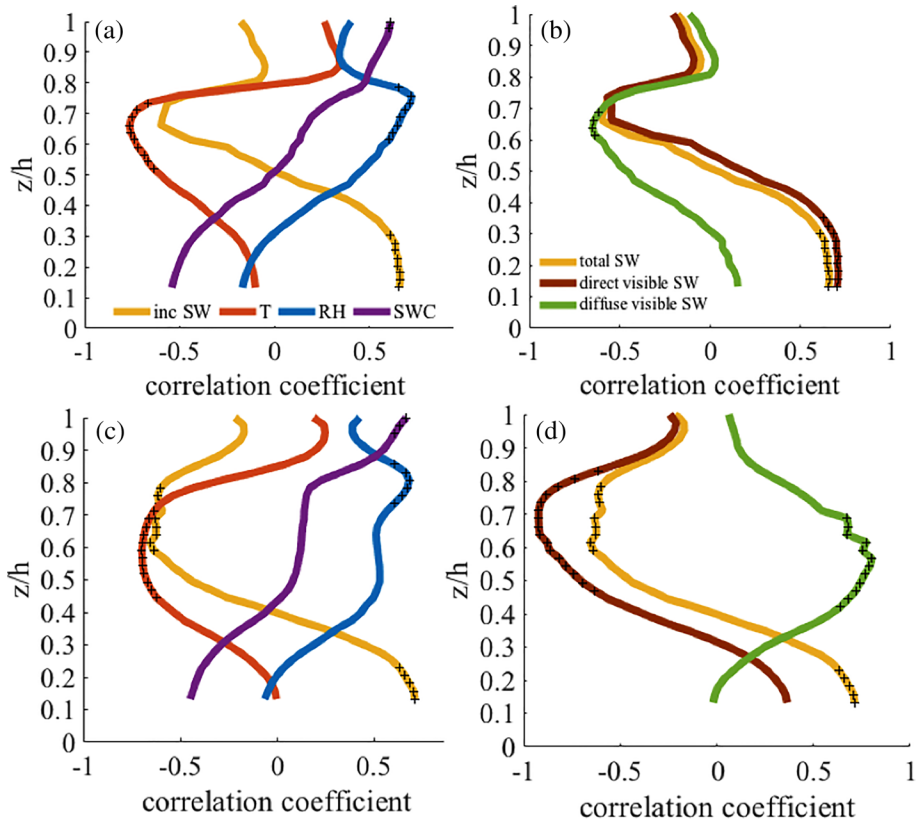

Figure 5. Correlation coefficients (as in Figure 4) for CLM-ml-SPA simulations at US-UMB, 2004–2014 using (a, b) parameterized diffuse visible light fraction. (c, d) Prescribed diffuse visible light fraction.

sensitivity of GPP to diffuse fraction is different for the prescribed diffuse simulation compared to the parameterized diffuse simulation and closer to the observed response of GPP to diffuse fraction (Figure 7). However, the positive response of GPP to diffuse fraction in CLM-ml shows a stronger gradient than observed (e.g., higher GPP with higher diffuse fractions), indicating that the model may be overestimating the impact of diffuse light on the DBF canopy (cf. Figure 7b with Figure 7c). Thus, the resulting increased dependence of midcanopy a_g should be considered with the knowledge that the model does not capture the observed diffuse light response.

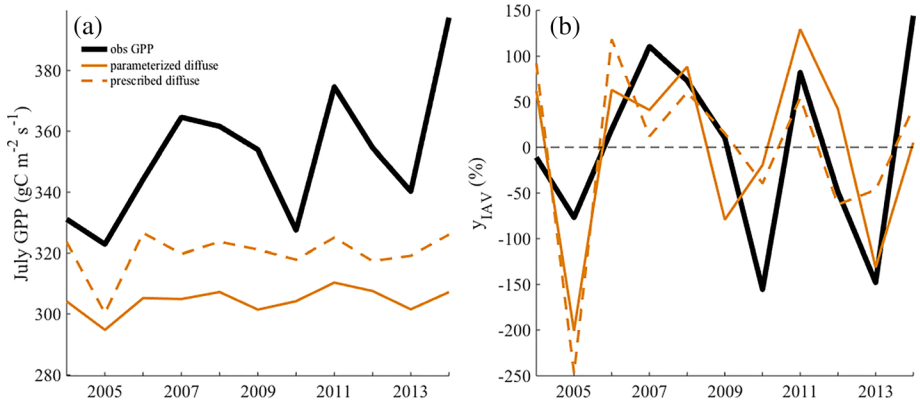

Figure 6. (a) Mean July GPP and (b) July GPP y_{IAV} for US-UMB comparing CLM-ml-SPA simulations using either parameterized (solid orange) or prescribed (dashed orange) diffuse fraction and observations.

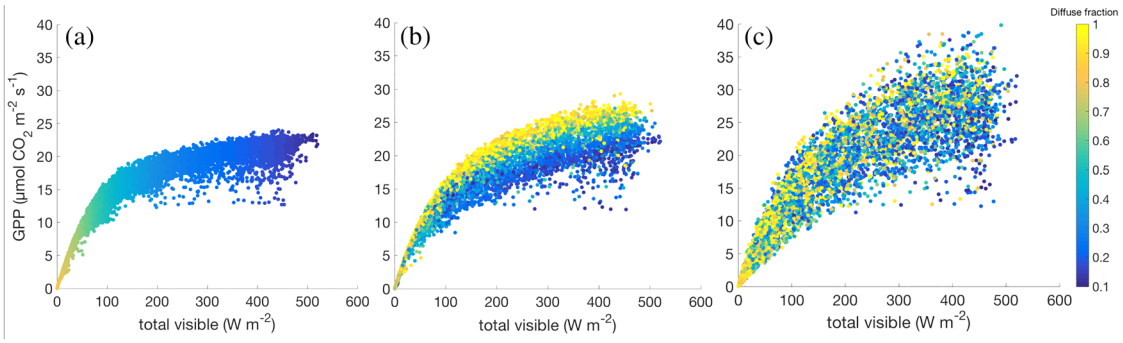

Figure 7. For the US-UMB site (2004–2014) and the CLM-ml-SPA, the total visible light intensity (W m^{-2}) at the top of the canopy versus the hourly simulated GPP, colored by diffuse light fraction (color bar) (a) parameterized diffuse fraction and (b) prescribed diffuse fraction. Panel (c) shows the observed relationship based on FLUXNET data.

3.5. Big-Leaf Plant Hydraulic Stress

As described in section 3.3, the use of the plant hydraulic stress parameterization in CLM-ml-SPA shows that within-canopy gradients can influence the GPP response. To see whether this result also applies to a big-leaf model, we compare two CLM5 simulations: one that uses soil moisture stress (e.g., Ball-Berry; CLM5-noPHS) and one that uses plant hydraulic stress (e.g., SPA; CLM5-PHS). The CLM5 analyses yield values of GPP S_{IAV} that are at some sites more similar to CLM4.5 and CLM-ml-BB (US-Ha1, US MMS, and US-UMB), and other sites more similar CLM-ml-SPA (US-Oho and US-WCr) (Figure 2 and Table S1). Both CLM5-PHS (PHS *on*) and CLM5-noPHS (PHS *off*) underestimate GPP magnitude more than the other simulations (Figure 2 and Table S1). CLM5-noPHSJuly mean GPP is somewhat lower than CLM5-PHS, but a previous study has shown these differences to be due to the default parameters in CLM for DBF and therefore not to the implementation of PHS (Franks et al., 2017). Overall, our results suggest that the CLM5 simulations do not improve the simulation of GPP magnitude and IAV with respect to FLUXNET observations relative to the other CLM simulations.

There is no clear impact of PHS in CLM5-PHS compared to CLM5-noPHSon the standard deviation of July GPP (S_{IAV}). At US-MMS and US-WCr, PHS decreased S_{IAV} (from 35.32 to 25.85 gC m^2 $month^{-1}$ and from 20.69 to 16.28 gC m^2 $month^{-1}$, respectively), while at US-Oho and US-UMB it increased S_{IAV} (from 7.36 to 9.2 gC m^2 $month^{-1}$ and from 25.55 to 38.35 gC m^2 $month^{-1}$, respectively). At US-Ha1, there was negligible difference (<1 gC m^2 $month^{-1}$). It should be noted that at US-MMS, US-Oho, and US-WCr, both CLM5 simulations (CLM5-PHS and CLM5-noPHS) showed decreased GPP IAV relative to that of CLM4.5, suggesting that a process other than PHS dampens GPP in the CLM5 model. The two CLM5 configurations are very similar when evaluating the regression coefficients between GPP and climate variables (Table 2). Thus, unlike the impacts of using SPA in CLM-ml instead of Ball-Berry and soil moisture stress, the use of PHS in CLM5 simulations did not have a large impact on GPP variability.

4. Discussion

Single-point runs at five DBF FLUXNET sites indicate that the default CLM4.5 underestimated both mean GPP and its IAV. Our comparison with CLM variants with more complex representations of canopy structure and/or mechanistically sound representations of the influence of soil moisture stress on the vegetation canopy suggests that these more sophisticated model structures did not improve GPP IAV relative to observations, as will be discussed below.

When comparing CLM-ml-BB simulations with CLM4.5 simulations, the multilayer canopy representation (including micrometeorological profiles, a leaf area profile, and explicit leaf layers) does not substantially impact GPP IAV or its response to interannual climate variability relative to a big-leaf scheme. Although simulations using CLM-ml-BB show vertical variation in carbon uptake, the difference in canopy-integrated GPP is negligible relative to CLM4.5. The lack of substantial vertical gradients in productivity could be due in part to the weak vertical microclimatic gradients in air temperature and RH in these simulations (Figures 1a

and 1b). A comparison of simulated and observed air temperature and RH gradients indicates that CLM-ml captures the qualities of the observed vertical variability in mean daytime temperature and RH profiles at US-UMB, although it tends to underestimate its within-canopy variability of air temperature by a half degree (~0.5°C in the model vs. 1°C in the observations) (Figure S5). Other studies have reported larger vertical micrometeorological variations of about 1–2°C (up to about 3°C in the case of the fir) throughout aspen, fir, and oak-hornbeam canopies (Eliáš et al., 1989; Flerchinger et al., 2015), so the effects of larger micrometeorological gradients may be stronger in other forest types. Another factor that could play a role in the weak vertical microclimatic variations is the leaf area distribution, as the CLM-ml prescribes a beta leaf area density (Figure 1e), and this may influence the microclimatic gradient. However, in a sensitivity test running CLM-ml-BB with a uniform leaf area among all layers, neither GPP IAV nor its regressions with climate IAV were different from simulations using the nonuniform distribution (not shown). Taken together, these results suggest that the multilayer representation in CLM-ml-BB does not influence the magnitude and IAV of GPP in deciduous forests compared to a big-leaf model.

While the role of temperature and atmospheric water vapor within a canopy did not have a strong impact, the role of leaf water and plant hydraulic stress did yield a stronger response in GPP in the multilayer model. When we replaced the Ball-Berry stomatal conductance with SPA, GPP IAV was dampened compared to CLM4.5 and CLM-ml-BB and altered the relationships between carbon uptake and climate IAV. The dampened IAV is traceable to the impact of plant hydraulic stress, which limits the impact of soil moisture stress to the uppermost canopy layers where radiation drives high transpiration and depletes leaf water (Figures 1c and 1d). The high transpiration rates in the upper leaf layers ($z/h > 0.6$) can only be maintained if adequate soil water is available to replenish their LWP, which often results in LWP falling below the threshold for stomata to remain open (−2 MPa). Meanwhile, there is less transpiration and water loss at lower leaf layers ($z/h < 0.6$), allowing these layers to maintain LWP above −1 MPa and to continue photosynthesizing even at low values of soil water (Figure S6). The result is that the midcanopy and lower canopy are not sensitive to soil moisture and thus yield a negative correlation with temperature and a positive correlation with radiation. As the lower canopy layers decouple from soil water limitation, their sensitivity to other drivers becomes more important and can result in sharp transitions in the sign of IAV within the canopy. Since these transitions usually occur in the upper half of the canopy where most of the leaf area is distributed (Figure 1e) and the impact on GPP is greatest, these sign transitions can result in canopy-integrated IAV near 0. The representation of alternatively water limited and temperature (or radiation) limited leaf layers and the cancelation between the a_g anomalies in these layers would not be captured by a single leaf layer. Thus, when SPA is used, the multilayer representation of the canopy significantly modifies IAV in GPP compared to the default model.

FLUXNET carbon fluxes (including partitioned fluxes like GPP) are subject to an ~20% random error (Richardson et al., 2006), and observational GPP IAV (up to ~10–15% of the mean, on average) is encompassed within that error range. Thus, the models' performance with respect to observed GPP IAV should be interpreted with caution. However, with respect to mean July GPP, all of the CLM variants have a negative bias relative to the observations well outside of the 20% error range. An analysis of hourly GPP at all sites shows that not a single model variant can simulate the highest values of GPP in the hourly observations (Figure 8). A previous analysis of FLUXNET data showed that hours with the highest GPP explained most of the IAV in annual GPP (Zscheischler et al., 2016), and the inability of the model to capture the upper range of variability may be one of the reasons that monthly scale GPP, and possibly its IAV, were not simulated accurately in this study. Our analyses in section 3.2 also showed that disturbances at some sites may have greatly impacted the regressions of GPP with climate drivers, implying that disturbances are an important source of error both in the flux observations as well as in the models (given that the models as configured here do not simulate disturbance events).

The representation of the IAV of hydrologic factors like soil moisture and evapotranspiration in CLM also show biases relative to observations (Figures S7 and S8). Soil moisture at all but one site (US-MMS) is either overestimated or underestimated and does not exhibit the same interannual pattern as in the observations (Figure S7). Like GPP, latent heat flux is predominantly underestimated by all model versions (Figure S8). Including plant hydraulics in CLM-ml and CLM5 increase mean latent heat exchange, improving some biases; however, where there was little bias in latent heat exchange simulated by CLM5-noPHS (US-WCr),

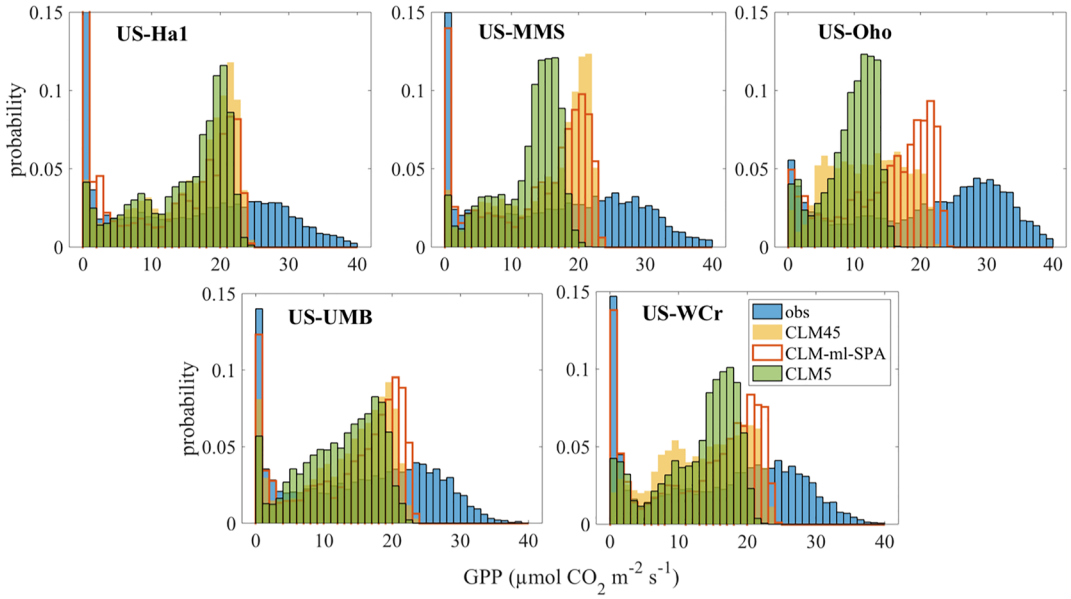

Figure 8. Histograms of daytime hourly GPP (GPP > 0) for FLUXNET observations and model simulations at all five study sites.

CLM-PHS overestimated latent heat exchange. Given that evapotranspiration is inherently linked to photosynthesis via stomatal opening in the model parameterizations, it is not surprising that these biases persist in the water budget. According to our regressions between GPP and soil moisture for the simulations and FLUXNET observations, CLM appears to overestimate the influence of soil moisture on GPP IAV when using traditional soil moisture stress, which might affect the timing of the positive and negative anomalies. However, it is unclear how simulated soil moisture may have affected the distribution of simulated hourly GPP. Two central pieces in model development leading from CLM4.5 to CLM5 were soil hydrology and plant hydraulics (Kennedy et al., 2019), which, like SPA, modulates photosynthesis via plant water status rather than soil water status. Using the eddy covariance observations as a constraint, our analysis suggests that plant hydraulics in CLM5, as well as SPA in CLM-ml, do not improve GPP variability relative to the observed range of GPP nor do they improve simulated GPP IAV. While improved vegetation and soil hydrological state and its coupling to carbon remain an important model development area, future modifications to stomatal conductance and photosynthesis in CLM should also address factors, or interactions among multiple factors, that contribute to periods of high GPP.

The influence of parametric uncertainty on modeled GPP IAV and magnitude could be an important component in disentangling model biases. Studies show that model parameters at single sites differ from default parameters utilized in global-scale simulation of PFTs (e.g., Post et al., 2018). Our study did not address the parametric uncertainty in these models at the selected study sites but instead focused on model structural differences. Additional model sensitivity studies would be required to fully explore the parameter space within the CLM model versions. By example, Figure S9 demonstrates the effects of varying parameter choices related to stomatal conductance and plant hydraulics on simulated July GPP at US-UMB and highlights the challenges at using parameteric changes to improve the simulation of GPP IAV. Selecting optimal parameters may not be straightforward or even productive, as Bonan et al. (2014) showed that optimizing these parameters alone for a single site may not lead to improved model representativeness given large uncertainty in optimal parameter values (see Figure 17 in Bonan et al., 2014).

In addition to the model structural and parametric uncertainties in vegetation and soil hydrology discussed above, the model-data discrepancy could be due to other canopy structural factors, as well as biophysical or biochemical processes not represented in this study. For example, leaf clumping (i.e., the tendency of leaves to overlap in "clumps") and leaf angle are both found to vary with height and enhance canopy response to the light environment. Several modeling studies show that clumping increases canopy carbon uptake,

primarily by increasing intercepted radiation in shaded leaves (Baldocchi & Harley, 1995; Chen et al., 2003; Walcroft et al., 2005). The carbon gains from leaf clumping (vs. randomly distributed leaves) is even greater when the vertical heterogeneity of leaf clumping is included (Walcroft et al., 2005). Another notable, vertically distributed canopy architectural trait is leaf angle, which may optimize trade-offs between radiation-induced leaf stresses and intercepted photosynthetic radiation and serve to increase carbon uptake in shaded leaves (Niinemets, 1998). Perhaps these architectural traits would serve to improve the models' negative biases. Vegetation phenology and pregrowing season climatological impacts, oversimplified by these models, could have affected simulated GPP IAV, as observational evidence shows that the seasonal maximum GPP (i.e., July GPP) in temperate forests exhibits lagged relationships to variability in spring climate and bud burst phenology (Baldocchi et al., 2018; Ouimette et al., 2018). Another study shows that forest stands that are older and/or exhibit higher species diversity tend to dampen IAV of net carbon uptake in forests, a feature that is not simulated in CLM (Musavi et al., 2017). Finally, coupled carbon-nitrogen biogeochemistry may greatly affect modeled responses of land carbon exchange to climate variability (Thornton et al., 2007), which could be especially important in the multilayer model setting since some deciduous forests have significant vertical variation in leaf nitrogen (Ellsworth & Reich, 1993).

5. Conclusions

The results of the multilayer canopy model simulations show that the influence of the multilayer canopy representation on simulated GPP IAV and its response to climate variability depended on the model stomatal conductance and water stress that was used. This result was consistent at five DBF sites with differing climates in the Northern United States. Among four soil moisture-limited sites (US-MMS, US-Oho, US-UMB, and US-WCr), CLM-ml simulations using Ball-Berry stomatal conductance showed that soil moisture was the dominant driver at all canopy layers, while radiation was the main driver at US-Ha1. Simulating vertically resolved LWP profiles and plant hydraulic stress at individual leaf layers (CLM-ml-SPA) dampens total GPP IAV due to a combination of the reduced impact of soil moisture and opposing leaf layer anomalies at different regimes in the canopy.

The simulated soil moisture response at the four soil moisture-limited sites was limited to the upper canopy layers, diminishing the overall impact of soil moisture on the canopy. Other drivers—temperature and radiation—take precedence in the middle and lower canopy leaf layers, altering the pattern of GPP IAV and ultimately dampening it. Because radiation IAV dominated the climatic influence on GPP IAV at US-Ha1, the particular moisture stress treatment (e.g., Ball-Berry or SPA) does not have an impact at this site. However, relative to FLUXNET observations, CLM-ml-SPA has a larger bias with observations than models without vertically resolved leaf water stress with respect to GPP IAV magnitude and y_{IAV}. Despite the realism when simulating plant hydraulic stress, a multilayer canopy representation does not make gains in terms of representativeness of the observations. The same GPP IAV dampening was not observed between single-layer canopy simulations of CLM5 with and without plant hydraulic stress, indicating that the dampening was unique to the multilayer implementation. However, it cannot be certain whether the dampening in the multilayer model was because stomatal conductance in SPA is designed to optimize water use efficiency, which differs from the empirical stomatal conductance in Ball-Berry, or because water stress varied by leaf layer.

Additionally, it was also shown that on diffuse light effects on canopy carbon uptake did not improve the simulation of GPP IAV, although it did cause the midcanopy to become more sensitive to SW radiation. Forcing model simulations with observed diffuse fraction slightly increased the magnitude of simulated carbon uptake, which is more consistent with observations. However, the overall impact of diffuse light in the model was not consistent with observations and model-predicted diffuse effect when prescribing observed diffuse fraction was considerably overestimated relative to the observed diffuse effect. Future work is needed to ensure that diffuse light impacts on canopy carbon uptake are accurately modeled with respect to observations.

Understanding the evolution of the terrestrial carbon sink is critical to the carbon balance in the atmosphere and the mitigation of anthropogenic climate change, and this study attempts to use a model to delineate the response of individual terrestrial carbon processes to climate variability. Our analysis shows that CLM4.5, CLM5, and CLM-ml all grossly underestimate GPP at midlatitude DBF FLUXNET sites and underestimate

the GPP response to climate variability. We show that increasing the complexity of the canopy structure to better capture vegetation-atmosphere coupling does not ameliorate model deficiencies nor does increasing the complexity of the moisture stress function within the model. In fact, adding these two changes together damps overall GPP variability as described above. Together, these results suggest that adding complexity in the canopy structure is alone not sufficient to resolve the fundamental biases that are present when models simulate the variability of carbon uptake, especially with outstanding parametric uncertainty, and that attention to the environmental drivers that influence variability is still required.

Conflict of Interest

The authors declare no competing interests.

Data Availability Statement

Model simulation data can be found on University of Michigan's Deep Blue data repository (at https://doi.org/10.7302/scmk-rf50).

Acknowledgments
We would like to thank NASA Interdisciplinary Science and Terrestrial Ecology for funding this work via Grant NNX17AK19G. The National Center for Atmospheric Research is a major facility sponsored by the National Science Foundation under Cooperative Agreement 1852977. We thank the FLUXNET2015 data set contributors for acquiring, maintaining, and providing data used in this study, specifically Chris Vogel at University of Michigan Biological Station for providing additional meteorological data for US-UMB, as well as site PIs and data managers for communicating site disturbances. We additionally thank Thiago Dos Santos for providing single-point CLM5 simulations and Zachary Butterfield for editorial advice.

References

Ahlström, A., Raupach, M. R., Schurgers, G., Smith, B., Arneth, A., Jung, M., et al. (2015). The dominant role of semi-arid ecosystems in the trend and variability of the land CO_2 sink. *Science*, *348*(6237), 895–899. https://doi.org/10.1126/science.aaa1668

Anav, A., Friedlingstein, P., Beer, C., Ciais, P., Harper, A., Jones, C., et al. (2015). Spatiotemporal patterns of terrestrial gross primary production: A review. *Reviews of Geophysics*, *53*, 785–818. https://doi.org/10.1002/2015RG000483

Anav, A., Friedlingstein, P., Kidston, M., Bopp, L., Ciais, P., Cox, P., et al. (2013). Evaluating the land and ocean components of the global carbon cycle in the CMIP5 Earth System Models. *Journal of Climate*, *26*(18), 6801–6843. https://doi.org/10.1175/JCLI-D-12-00417.1

Aranda, I., Cano, F. J., Gasco, A., Cochard, H., Nardini, A., Mancha, J. A., et al. (2015). Variation in photosynthetic performance and hydraulic architecture across European beech (*Fagus sylvatica L.*) populations supports the case for local adaptation to water stress. *Tree Physiology*, *35*(1), 34–46. https://doi.org/10.1093/treephys/tpu101

Arora, V. K., Boer, G. J., Friedlingstein, P., Eby, M., Jones, C. D., Christian, J. R., et al. (2013). Carbon-concentration and carbon-climate feedbacks in CMIP5 Earth system models. *Journal of Climate*, *26*(15), 5289–5314. https://doi.org/10.1175/JCLI-D-12-00494.1

Baldocchi, D., Chu, H., & Reichstein, M. (2018). Inter-annual variability of net and gross ecosystem carbon fluxes: A review. *Agricultural and Forest Meteorology*, *249*, 520–533. https://doi.org/10.1016/j.agrformet.2017.05.015

Baldocchi, D. D., & Harley, P. C. (1995). Scaling carbon dioxide and water vapour exchange from leaf to canopy in a deciduous forest. II. Model testing and application. *Plant, Cell & Environment*, *18*(10), 1157–1173. https://doi.org/10.1111/j.1365-3040.1995.tb00626.x

Baldocchi, D. D., Wilson, K. B., & Gu, L. (2002). How the environment, canopy structure and canopy physiological functioning influence carbon, water and energy fluxes of a temperate broad-leaved deciduous forest—An assessment with the biophysical model CANOAK. *Tree Physiology*, *22*(15–16), 1065–1077. https://doi.org/10.1093/treephys/22.15-16.1065

Beer, C., Reichstein, M., Tomelleri, E., Ciais, P., Jung, M., Carvalhais, N., et al. (2010). Terrestrial gross carbon dioxide uptake: Global distribution and covariation with climate. *Science*, *329*(5993), 834–838. https://doi.org/10.1126/science.1184984

Bonan, G. B., & Doney, S. C. (2018). Climate, ecosystems, and planetary futures: The challenge to predict life in earth system models. *Science*, *359*(6375), eaam8328.

Bonan, G. B., Patton, E. G., Harman, I. N., Oleson, K. W., Finnigan, J. J., Lu, Y., & Burakowski, E. A. (2018). Modeling canopy-induced turbulence in the Earth system: A unified parameterization of turbulent exchange within plant canopies and the roughness sublayer (CLM-ml v0). Geoscientific Model Development.

Bonan, G. B., Williams, M., Fisher, R. A., & Oleson, K. W. (2014). Modeling stomatal conductance in the Earth system: Linking leaf water-use efficiency and water transport along the soil-plant-atmosphere continuum. *Geoscientific Model Development*, *7*(5), 2193–2222. https://doi.org/10.5194/gmd-7-2193-2014

Carlson, D. W., & Groot, A. (1997). Microclimate of clear-cut, forest interior, and small openings in trembling aspen forest. *Agricultural and Forest Meteorology*, *87*(4), 313–329. https://doi.org/10.1016/S0168-1923(95)02305-4

Chang, K. Y., & Chen, S. H. (2018). Canopy profile sensitivity on surface layer simulations evaluated by a multiple canopy layer higher order closure land surface model. *Agricultural and Forest Meteorology*, *252*, 192–207. https://doi.org/10.1016/j.agrformet.2018.01.027

Chen, J., Saunders, S. C., Crow, T. R., Naiman, R. J., Brosofske, K. D., Mroz, G. D., et al. (1999). Microclimate in forest ecosystem and landscape ecology: Variations in local climate can be used to monitor and compare the effects of different management regimes. *Bioscience*, *49*(4), 288–297. https://doi.org/10.2307/1313612

Chen, J. M., Liu, J., Leblanc, S. G., Lacaze, R., & Roujean, J.-L. (2003). Multi-angular optical remote sensing for assessing vegetation structure and carbon absorption. *Remote Sensing of Environment*, *84*(4), 516–525. https://doi.org/10.1016/S0034-4257(02)00150-5

Cheng, S. J., Bohrer, G., Steiner, A. L., Hollinger, D. Y., Suyker, A., Phillips, R. P., & Nadelhoffer, K. J. (2015). Variations in the influence of diffuse light on gross primary productivity in temperate ecosystems. *Agricultural and Forest Meteorology*, *201*, 98–110. https://doi.org/10.1016/j.agrformet.2014.11.002

Collatz, G. J., Ball, J. T., Grivet, C., & Berry, J. A. (1991). Physiological and environmental regulation of stomatal conductance, photosynthesis and transpiration: A model that includes a laminar boundary layer. *Agricultural and Forest Meteorology*, *54*(2–4), 107–136. https://doi.org/10.1016/0168-1923(91)90002-8

de Frenne, P., Rodriguez-Sanchez, F., Coomes, D. A., Baeten, L., Verstraeten, G., Vellend, M., et al. (2013). Microclimate moderates plant responses to macroclimate warming. *Proceedings of the National Academy of Sciences*, *110*(46), 18,561–18,565. https://doi.org/10.1073/pnas.1311190110

Desai, A. R. (2010). Climatic and phenological controls on coherent regional interannual variability of carbon dioxide flux in a heterogeneous landscape. *Journal of Geophysical Research*, *115*, G00J02. https://doi.org/10.1029/2010JG001423

Drewry, D. T., Kumar, P., Long, S., Bernacchi, C., Liang, X. Z., & Sivapalan, M. (2010). Ecohydrological responses of dense canopies to environmental variability: 1. Interplay between vertical structure and photosynthetic pathway. *Journal of Geophysical Research*, *115*, G04022. https://doi.org/10.1029/2010JG001340

Eliáš, P., Kratochvílová, I., Janouš, D., Marek, M., & Masarovičová, E. (1989). Stand microclimate and physiological activity of tree leaves in an oak-hornbeam forest. *Trees*, *3*(4), 227–233. https://doi.org/10.1007/BF00225356

Ellsworth, D. S., & Reich, P. B. (1993). Canopy structure and vertical patterns of photosynthesis and related leaf traits in a deciduous forest. *Oecologia*, *96*(2), 169–178. https://doi.org/10.1007/BF00317729

Farquhar, G. D., von Caemmerer, S. V., & Berry, J. A. (1980). A biochemical model of photosynthetic CO_2 assimilation in leaves of C_3 species. *Planta*, *149*(1), 78–90. https://doi.org/10.1007/BF00386231

Flerchinger, G. N., Reba, M. L., Link, T. E., & Marks, D. (2015). Modeling temperature and humidity profiles within forest canopies. *Agricultural and Forest Meteorology*, *213*, 251–262. https://doi.org/10.1016/j.agrformet.2015.07.007

Franks, P. J., Berry, J. A., Lombardozzi, D. L., & Bonan, G. B. (2017). Stomatal function across temporal and spatial scales: Deep-time trends, land-atmosphere coupling and global models. *Plant Physiology*, *174*(2), 583–602. https://doi.org/10.1104/pp.17.00287

Fu, Z., Dong, J., Zhou, Y., Stoy, P. C., & Niu, S. (2017). Long term trend and interannual variability of land carbon uptake—The attribution and processes. *Environmental Research Letters*, *12*(1), 014018. https://doi.org/10.1088/1748-9326/aa5685

Funk, J. L., & Lerdau, M. T. (2004). Photosynthesis in forest canopies. *Forest canopies*, *2*, 335–358.

Gu, L., Baldocchi, D., Verma, S. B., Black, T. A., Vesala, T., Falge, E. M., & Dowty, P. R. (2002). Advantages of diffuse radiation for terrestrial ecosystem productivity. *Journal of Geophysical Research*, *107*(D6), ACL 2–1. https://doi.org/10.1029/2001jd001242

Hellkvist, J., Richards, G., & Jarvis, P. G. (1974). Vertical gradients of water potential and tissue water relations in Sitka spruce trees measured with the pressure chamber. *Journal of Applied Ecology*, *11*(2), 637. https://doi.org/10.2307/2402215

Keeling, C. D., Whorf, T. P., Wahlen, M., & van der Plichtt, J. (1995). Interannual extremes in the rate of rise of atmospheric carbon dioxide since 1980. *Nature*, *375*(6533), 666–670. https://doi.org/10.1038/375666a0

Keenan, T. F., Baker, I., Barr, A., Ciais, P., Davis, K., Dietze, M., et al. (2012). Terrestrial biosphere model performance for inter-annual variability of land-atmosphere CO_2 exchange. *Global Change Biology*, *18*(6), 1971–1987. https://doi.org/10.1111/j.1365-2486.2012.02678.x

Kennedy, D., Swenson, S., Oleson, K. W., Lawrence, D. M., Fisher, R., Lola da Costa, A. C., & Gentine, P. (2019). Implementing plant hydraulics in the Community Land Model, Version 5. *Journal of Advances in Modeling Earth Systems*, *11*, 485–513. https://doi.org/10.1029/2018MS001500

Koike, T., Kitao, M., Maruyama, Y., Mori, S., & Lei, T. T. (2001). Leaf morphology and photosynthetic adjustments among deciduous broad-leaved trees within the vertical canopy profile. *Tree Physiology*, *21*(12–13), 951–958. https://doi.org/10.1093/treephys/21.12-13.951

Lasslop, G., Migliavacca, M., Bohrer, G., Reichstein, M., Bahn, M., Ibrom, A., et al. (2012). On the choice of the driving temperature for eddy-covariance carbon dioxide flux partitioning. *Biogeosciences*, *9*(12), 5243–5259. https://doi.org/10.5194/bg-9-5243-2012

Lawrence, D. M., Fisher, R. A., Koven, C. D., Oleson, K. W., Swenson, S. C., Bonan, G., et al. (2019). The Community Land Model Version 5: Description of new features, benchmarking, and impact of forcing uncertainty. *Journal of Advances in Modeling Earth Systems*, *11*, 4245–4287. https://doi.org/10.1029/2018MS001583

Lawrence, P. J., & Chase, T. N. (2007). Representing a new MODIS consistent land surface in the Community Land Model (CLM 3.0). *Journal of Geophysical Research*, *112*, G01023. https://doi.org/10.1029/2006JG000168

le Quéré, C., Andrew, R. M., Friedlingstein, P., Sitch, S., Pongratz, J., Manning, A. C., et al. (2017). Global carbon budget 2017. *Earth System Science Data Discussions*, 1–79.

Medlyn, B. E., Duursma, R. A., Eamus, D., Ellsworth, D. S., Prentice, I. C., Barton, C. V., et al. (2011). Reconciling the optimal and empirical approaches to modelling stomatal conductance. *Global Change Biology*, *17*(6), 2134–2144. https://doi.org/10.1111/j.1365-2486.2010.02375.x

Murray, F. W. (1967). On the computation of saturation vapor pressure. *Rand Corp Santa Monica California*, (P-3423).

Musavi, T., Migliavacca, M., Reichstein, M., Kattge, J., Wirth, C., Black, T. A., et al. (2017). Stand age and species richness dampen inter-annual variation of ecosystem-level photosynthetic capacity. *Nature ecology & evolution*, *1*(2), 0048. https://doi.org/10.1038/s41559-016-0048

Nevison, C. D., Mahowald, N. M., Doney, S. C., Lima, I. D., van der Werf, G. R., Randerson, J. T., et al. (2008). Contribution of ocean, fossil fuel, land biosphere, and biomass burning carbon fluxes to seasonal and interannual variability in atmospheric CO2. *Journal of Geophysical Research*, *113*, G01010. https://doi.org/10.1029/2007JG000408

Niinemets, Ü. (1998). Adjustment of foliage structure and function to a canopy light gradient in two co-existing deciduous trees. Variability in leaf inclination angles in relation to petiole morphology. *Trees*, *12*(7), 446–451. https://doi.org/10.1007/s004680050173

Niinemets, Ü., & Valladares, F. (2004). Photosynthetic acclimation to simultaneous and interacting environmental stresses along natural light gradients: Optimality and constraints. *Plant Biology*, *6*(3), 254–268. https://doi.org/10.1055/s-2004-817881

Niyogi, D. (2004). Direct observations of the effects of aerosol loading on net ecosystem CO_2 exchanges over different landscapes. *Geophysical Research Letters*, *31*(20). https://doi.org/10.1029/2004gl020915

Oleson, K. W., Lawrence, D. M., Bonan, G. B., Drewniack, B., Huang, M., Koven, C. D., et al. (2013). *Technical description of version 4.5 of the Community Land Model (CLM)* (Technical Note No. NCAR/TN-503+ STR). Boulder, CO: National Center for Atmospheric Research Earth System Laboratory.

Ouimette, A. P., Ollinger, S. V., Richardson, A. D., Hollinger, D. Y., Keenan, T. F., Lepine, L. C., & Vadeboncoeur, M. A. (2018). Carbon fluxes and interannual drivers in a temperate forest ecosystem assessed through comparison of top-down and bottom-up approaches. *Agricultural and Forest Meteorology*, *256*, 420–430.

Pan, Y., Birdsey, R. A., Fang, J., Houghton, R., Kauppi, P. E., Kurz, W. A., et al. (2011). A large and persistent carbon sink in the world's forests. *Science*, *333*(6045), 988–993. https://doi.org/10.1126/science.1201609

Parker, G., Tinoco-Ojanguren, C., Martínez-Yrízar, A., & Maass, M. (2005). Seasonal balance and vertical pattern of photosynthetically active radiation within canopies of a tropical dry deciduous forest ecosystem in Mexico. *Journal of Tropical Ecology*, *21*(3), 283–295. https://doi.org/10.1017/S0266467405002282

Parker, G. G., O'Neill, J. P., & Higman, D. (1989). Vertical profile and canopy organization in a mixed deciduous forest. *Vegetatio*, *85*(1–2), 1–11. https://doi.org/10.1007/BF00042250

Pastorello, G., Papale, D., Chu, H., Trotta, C., Agarwal, D., Canfora, E., et al. (2017). A new data set to keep a sharper eye on land-air exchanges. *Eos, Transactions American Geophysical Union (Online)*, *98*(8).

Post, H., Hendricks Franssen, H.-J., Han, X., Baatz, R., Montzka, C., Schmidt, M., & Vereecken, H. (2018). Evaluation and uncertainty analysis of regional-scale CLM4.5 net carbon flux estimates. *Biogeosciences*, *15*(1), 187–208. https://doi.org/10.5194/bg-15-187-2018

Poulter, B., Frank, D., Ciais, P., Myneni, R. B., Andela, N., Bi, J., et al. (2014). Contribution of semi-arid ecosystems to interannual variability of the global carbon cycle. *Nature*, *509*(7502), 600–603. https://doi.org/10.1038/nature13376

Rambo, T. R., & North, M. P. (2009). Canopy microclimate response to pattern and density of thinning in a Sierra Nevada forest. *Forest Ecology and Management*, *257*(2), 435–442. https://doi.org/10.1016/j.foreco.2008.09.029

Richardson, A. D., Hollinger, D. Y., Burba, G. G., Davis, K. J., Flanagan, L. B., Katul, G. G., et al. (2006). A multi-site analysis of random error in tower-based measurements of carbon and energy fluxes. *Agricultural and Forest Meteorology*, *136*(1–2), 1–18. https://doi.org/10.1016/j.agrformet.2006.01.007

Rödenbeck, C., Zaehle, S., Keeling, R., & Heimann, M. (2018). How does the terrestrial carbon exchange respond to inter-annual climatic variations? *Biogeosciences*, *15*(8), 2481–2498. https://doi.org/10.5194/bg-15-2481-2018

Schimel, D. S., House, J. I., Hibbard, K. A., Bousquet, P., Ciais, P., Peylin, P., et al. (2001). Recent patterns and mechanisms of carbon exchange by terrestrial ecosystems. *Nature*, *414*(6860), 169–172. https://doi.org/10.1038/35102500

Shiga, Y. P., Michalak, A. M., Fang, Y., Schaefer, K., Andrews, A. E., Huntzinger, D. H., et al. (2018). Forests dominate the interannual variability of the North American carbon sink. *Environmental Research Letters*, *13*(8), 084015. https://doi.org/10.1088/1748-9326/aad505

Sinclair, T. R., Murphy, C. E., & Knoerr, K. R. (1976). Development and evaluation of simplified models for simulating canopy photosynthesis and transpiration. *Journal of Applied Ecology*, *13*(3), 813. https://doi.org/10.2307/2402257

Sitch, S., Friedlingstein, P., Gruber, N., Jones, S. D., Murray-Tortarolo, G., Ahlström, A., et al. (2015). Recent trends and drivers of regional sources and sinks of carbon dioxide. *Biogeosciences*, *12*(3), 653–679. https://doi.org/10.5194/bg-12-653-2015

Taylor, D., & Eamus, D. (2008). Coordinating leaf functional traits with branch hydraulic conductivity: Resource substitution and implications for carbon gain. *Tree Physiology*, *28*(8), 1169–1177. https://doi.org/10.1093/treephys/28.8.1169

Thornton, P. E., Lamarque, J. F., Rosenbloom, N. A., & Mahowald, N. M. (2007). Influence of carbon-nitrogen cycle coupling on land model response to CO_2 fertilization and climate variability. *Global Biogeochemical Cycles*, *21*, GB4018. https://doi.org/10.1029/2006GB002868

Tyree, M. T., & Ewers, F. W. (1991). The hydraulic architecture of trees and other woody plants. *New Phytologist*, *119*(3), 345–360. https://doi.org/10.1111/j.1469-8137.1991.tb00035.x

von Arx, G., Dobbertin, M., & Rebetez, M. (2012). Spatio-temporal effects of forest canopy on understory microclimate in a long-term experiment in Switzerland. *Agricultural and Forest Meteorology*, *166*, 144–155.

Walcroft, A. S., Brown, K. J., Schuster, W. S. F., Tissue, D. T., Turnbull, M. H., Griffin, K. L., & Whitehead, D. (2005). Radiative transfer and carbon assimilation in relation to canopy architecture, foliage area distribution and clumping in a mature temperate rainforest canopy in New Zealand. *Agricultural and Forest Meteorology*, *135*(1-4), 326–339. https://doi.org/10.1016/j.agrformet.2005.12.010

Williams, M., Bond, B. J., & Ryan, M. G. (2001). Evaluating different soil and plant hydraulic constraints on tree function using a model and sap flow data from ponderosa pine. *Plant, Cell & Environment*, *24*(7), 679–690. https://doi.org/10.1046/j.1365-3040.2001.00715.x

Williams, M., Rastetter, E. B., Fernandes, D. N., Goulden, M. L., Wofsy, S. C., Shaver, G. R., et al. (1996). Modelling the soil-plant-atmosphere continuum in a Quercus-Acer stand at Harvard Forest: The regulation of stomatal conductance by light, nitrogen and soil/plant hydraulic properties. *Plant, Cell & Environment*, *19*(8), 911–927. https://doi.org/10.1111/j.1365-3040.1996.tb00456.x

Williams, M., Richardson, A. D., Reichstein, M., Stoy, P. C., Peylin, P., Verbeeck, H., et al. (2009). Improving land surface models with FLUXNET data. *Biogeosciences*, *6*(7), 1341–1359. https://doi.org/10.5194/bg-6-1341-2009

Wu, Y., Brashers, B., Finkelstein, P. L., & Pleim, J. E. (2003). A multilayer biochemical dry deposition model 2. Model evaluation. *Journal of Geophysical Research*, *108*(D1), 4014. https://doi.org/10.1029/2002JD002306

Zeng, X., & Dickinson, R. E. (1998). Effect of surface sublayer on surface skin temperature and fluxes. *Journal of Climate*, *11*(4), 537–550. https://doi.org/10.1175/1520-0442(1998)011<0537:EOSSOS>2.0.CO;2

Zhang, J.-L., & Cao, K.-F. (2009). Stem hydraulics mediates leaf water status, carbon gain, nutrient use efficiencies and plant growth rates across dipterocarp species. *Functional Ecology*, *23*(4), 658–667. https://doi.org/10.1111/j.1365-2435.2009.01552.x

Zhao, F., Yang, X., Schull, M. A., Román-Colón, M. O., Yao, T., Wang, Z., et al. (2011). Measuring effective leaf area index, foliage profile, and stand height in New England forest stands using a full-waveform ground-based lidar. *Remote Sensing of Environment*, *115*(11), 2954–2964. https://doi.org/10.1016/j.rse.2010.08.030

Zscheischler, J., Fatichi, S., Wolf, S., Blanken, P. D., Bohrer, G., Clark, K., et al. (2016). Short-term favorable weather conditions are an important control of interannual variability in carbon and water fluxes. *Journal of Geophysical Research: Biogeosciences*, *121*, 2186–2198. https://doi.org/10.1002/2016JG003503